Egyptian Journal of Chemistry

http://ejchem.journals.ekb.eg/

Manganese, Cobalt, and Cadmium Complexes of Quinazoline Schiff Base Ligand and Methionine: Synthesis, Characterization, DFT, Docking studies and biomedical application

M.S.A. Mansour*, Abeer Taha Ibrahium, Ahmed A. El-Sherif1, Walaa H. Mahmoud

Chemistry Department, Faculty of Science, Cairo University, Giza, 12613 Egypt

Abstract

Mixed ligand complexes of Mn[II], Co[II] and Cd[II] with a novel Schiff base ligand 4-(2-((1E,2E)-1-(2-(p-tolyl)hydrazineylidene)propan-2-ylidene)hydrazineyl) as principal ligand (**L_1**) and Methionine (**L_2**) as an ancillary ligand were successfully synthesized and thoroughly characterized by employing various analytical methods, including Elemental analysis, FT-IR, UV-Visible, Mass spectra, and conductometric measurements. Density functional theory (DFT) computations have being executed employing LANL2DZ basis sets, conjoined with the B3LYP correlation functional, to elucidate the stable electronic configuration, (HOMO–LUMO) energy gap, dipole moment, and chemical hardness of the hybrid ligand complexes. The proposed geometry for the complexes is a distorted octahedral structure. Additionally, the structural parameters and (MEP) Molecular Electrostatic Potential of these compounds were calculated using a DFT level basis set and allied with the experimental records. The antimicrobial potential of these compounds were assessed in contradiction of a diverse range of bacterial and fungal strains, encompassing Gram(+ve) bacteria such as *Streptococcus mutans* and *Staphylococcus aureus*, Gram(-ve) bacteria like *Klebsiella Pneumonia* and *Escherichia coli*, and the fungus *Candida albicans*. Significantly, these complexes demonstrated noteworthy antimicrobial activities, with the Cd (II) complex exhibiting the greatest efficacy against all the checked organisms. In the pursuit of exploring their broader medical potential, these compounds were also investigated for their antibiotic properties against *H. pylori*, showing substantial potential as effective antibiotics against this bacterium. Furthermore, the synthesized complexes were considered for their antitumor properties against MCF-7 [Breast carcinoma] cells. Among them, the **[(L_1) (L_2) Co (Cl)].3H_2O** complex displayed the most potent activity, with the lowest IC_{50} value of 17 µg/ml compared to cisplatin. Moreover, it exhibited reduced cytotoxicity towards normal cells (VERO cells) in comparison to cisplatin, establishing it as the supreme potent compound in the study. Moreover, molecular docking studies were conducted using DFT-optimized structures of the Schiff base ligand **(L_1)** and its Cd (II) complex to elucidate their interactions with selected protein structures involving **(3AHU, 1GHP, 2ZIC, 4N74, 5JPE, 3HB5, and 6W41),** providing insights into their preferred modes of interaction. This comprehensive study underscores the multifaceted applications and promising bioactive properties of these synthesized compounds.

KEYWORDS: Ternary metal complexes; spectral studies; ; Antimicrobial activity; H-Pylori; Breast cancer; COVID-19

1. Introduction

Mixed ligand complexes have garnered significant attention from researchers due to their profound relevance in biological systems, particularly in terms of their pharmacological properties. These complexes have demonstrated promising potential in a wide range of medicinal applications, including inhibiting neoplastic growth, combating bacterial and fungal infections, suppressing mycological proliferation, countering viral threats, mitigating inflammatory responses, regulating blood pressure, alleviating arthritic symptoms, providing analgesic effects, and reducing fever, while also displaying antibiotic properties [1–2]. Moreover, their utility extends beyond medicine to encompass catalytic activities in various chemical reactions, as well as applications in the food and dye industries, analytical chemistry, and biological modeling. Recent studies have specifically focused on mixed ligand complexes involving amino acids and aromatic amines with metal ions and their associated biological activities [3–4]. Out of the ninety, naturally occurring elements on Earth, eighty-one are conducive to supporting life, and sixty-one of

*Corresponding author e-mail: Adammidomansour@gmail.com (Mansour, Mohammad Saeid).
Received date 01 February 2024; revised date 12 March 2024; accepted date 14 March 2024
DOI: 10.21608/EJCHEM.2024.266673.9275

these are metals. Interestingly, our bodies contain approximately three percent of these metals. This connection between metals and life has led to growing clinical and commercial interest in metal complexes. Metal complexes, particularly inorganic ones, have been employed for the treatment of numerous diseases and ailments for many years. In the contemporary medical landscape, a substantial number of pharmaceutical agents belong to major classes that incorporate metal complexes are widely used in clinical settings [5]. The pivotal role of metal ions within these complexes lies in their ability to serve as templates for synthesis and introduce activities that enhance the delivery of drugs. This is significant because many organic drugs require interactions with metal ions to exhibit their therapeutic effects. Metal complexes offer unique structural scaffolds and possess the capacity to arrange surrounding atoms in ways not easily achievable through other means. Also, their effects can be highly specific, and they can be tailored to influence cellular processes that recognize specific types of metal-macromolecule interactions. In the context of mixed ligand complexes, ligands exert influence not only on the reactivity of metals but also significantly contribute to shaping secondary coordination sphere interactions. These interactions are pivotal in recognizing and discerning biological target sites such as DNA, enzymes, and protein receptors. [6–7]. DL-methionine, a sulfur-containing amino acid, serves as a secondary ligand in the creation of mixed ligands metal complexes. Methionine is essential for various physiological functions, including immunity, metabolism, oxidation, and protein production. Unlike other proteins synthesized by the human body [8, 9], methionine is classified as essential and plays a unique role due to its sulfur content. It is crucial for normal mammalian growth [10] and aids in reducing liver fat deposition. Additionally, methionine contributes to cartilage tissue therapy [11, 12]. Metabolized into homocysteine, it participates in biochemical processes, such as methyl donation, DNA stabilization, and protein protection [13]. Methionine acts as a precursor for S-adenosylmethionine, facilitating methyl transfer in various enzymatic activities, including RNA, DNA, and protein modification [14, 15]. Discovered in 1982 within the lining of the human stomach, *Helicobacter pylori* is a corkscrew-shaped bacterium that classified within the Gram(-ve) group. Its presence in the stomach can lead to various digestive problems, including persistent active inflammation of the stomach lining, symptoms of indigestion, as well as the development of ulcers in both the gastric and duodenal regions. Moreover, this bacterium is associated with the development of serious conditions like lymphoma affecting the B cells in the mucosa-associated lymphoid tissue (MALT) of the stomach and adenocarcinoma in the gastric region. [16]. Beyond its impact on the stomach, *H. pylori* infection has been connected to a range of other health complications, involving idiopathic thrombocytopenic purpura, deficiencies in iron and vitamin B_{12}, coronary artery disease, various neurodegenerative disorders, and problems related to the gallbladder like cholecystitis and cholelithiasis [16]. This study endeavors to generate a new Schiff base ligand (L1) by combining (E)-1-(2-(p-tolyl)hydrazineylidene) propan-2-one with 4hydrazineylquinazoline. Subsequently, the goal is to form mixed ligand complexes by incorporating a new Schiff base ligand (L_1), methionine ligand (L_2) and transition metals such as Mn (II), Co (II) and Cd (II). The characterization process involves employing various physico-chemical techniques. The research covers an exploration of biological functionalities, including antibacterial, antifungal, and anticancer attributes of both the Schiff base (L_1) and its ternary metal complexes. Moreover, the enquiry aims to assess the possible inhibitory influences of the Schiff base (L_1) and its metal complexes on *H. pylori* infection. Additionally, research involved molecular docking investigations aimed at understanding the potential binding mechanisms of Schiff base ligand (L_1) and its Cd(II) complex within the active sites of several receptors (**3AHU, 1GHP, 2ZIC, 4N74, 5JPE, 3HB5**, and **6W41**). The docking analyses were performed using the MOE software, which is well-known for its inflexible molecular docking capabilities. The optimization of the Schiff base ligand (L_1) and its Cd (II) complex was carried out by applying the DFT-based B3LYP technique. This method utilized the LANL2DZ basis set for both the Schiff base ligand and its associated metal complexes.

2. Materials and methods

2.1. Experimental

2.1.1. Chemicals and reagents.

This study employed high-purity chemicals, such as 4-hydrazinoquinazoline and (E)-1-(2-(p-tolyl)hydrazinylidene)propan-2-one purchased from Merck, $MnCl_2.4H_2O$ obtained from BDH and both $CoCl_2.6H_2O$ and $CdCl_2.2H_2O$ from Sigma Aldrich. Methionine was sourced from Merck. Absolute Ethanol, a spectroscopically pure organic solvent, was acquired from BDH. Bidistilled water from glass apparatus was consistently managed in all preparations. The MCF-7 human tumor cell line, originally stored at -180°C in liquid nitrogen, was obtained from the American Type Culture Collection. Through successive sub-culturing, the cultivation and maintenance of the MCF-7 tumor cell line were performed at the National Cancer Institute in Cairo, Egypt.

2.1.2. Solutions

Solution reservoirs containing Schiff base ligand (**L_1**) and its metal complexes were prepared at a predetermined concentration level of 1 X 10^{-3} M. This was achieved by accurately dissolving the appropriate amount of each compound in N,N-dimethylformamide. To assess the conductivity, the 1 X 10^{-3} M metal complex solution was examined. Subsequently, for UV–Vis spectra measurement, we created diluted solutions of the Schiff base quinazoline ligand(L_1) and its metal complexes at a predetermined concentration of 1 X 10^{-4} M by carefully diluting them from the previously made stock solutions.

2.1.3. Resolution of Anti-Helicobacter Pylori Investigation

2.1.3.1. Creating Bacterial Suspensions: A Step-by-Step Guide

To create an inoculum for the susceptibility tests, colonies of the microorganisms were transferred into tubes with sterile physiological saline solution. The turbidity was adjusted to match the 2.0 McFarland standard by ensuring the suspension reached a specific density. This turbidity level generates a suspension roughly equivalent to 1.0 x 10^8 colony-forming units per milliliter (CFU/mL) of *H. pylori*, as per prior references [17].

2.1.3.2. Assessing the Efficacy of Agents against H. Pylori Infection.

The examination of the anti-H. Pylori properties in vitro was conducted using the well agar diffusion method [17, 18]. In summary, 100 µl of an H. pylori suspension (1.0 × 10^8 CFUs/ml) was evenly distributed on Mueller Hinton agar plates (BBL) supplemented with 10% sheep blood. Subsequently, a sterile cork borer or tip was used to aseptically create a hole measuring 6 to 8 mm in diameter. Following this, 100 µl of the antimicrobial agent or extract solution at the desired concentration was introduced into the well. For the negative control, DMSO was utilized, while the positive controls comprised antibiotics such as amoxicillin (AMX, 0.05 mg/ml), clarithromycin (CLR, 0.05 mg/ml), and metronidazole (MTZ, 0.8 mg/ml). The plates were then incubated for 72 hours at 37°C under microaerophilic conditions with humidity. Finally, the diameter of the inhibition zone was measured [18].

2.1.4. Solution of anticancer study

A freshly prepared stock solution of the Schiff base ligand (L_1) at a concentration of 1 × 10^{-3} M was created in ethanol (90%) to make an appropriate volume. For cell cryopreservation, dimethyl sulfoxide (DMSO) was used, and the RPMI-1640 medium, employed for the culture and maintenance of a human tumor cell line, was prepared from its powder form. This was done by mixing 10.40 g of medium with 2 g of sodium bicarbonate, making the final volume up to 1 liter with distilled water, and ensuring complete dissolution through gentle agitation. The medium was then sterilized via filtration using a 0.22 µm Millipore bacterial filter, stored at 4°C, and regularly checked for any signs of contamination. Prior to application, the RPMI-1640 medium was preheated to 37°C using a water bath and enriched with penicillin-streptomycin and fetal bovine serum (FBS). ($NaHCO_3$) Sodium bicarbonate played a crucial role in the formulation of the RPMI-1640 medium. A 0.05% isotonic trypan blue solution was prepared in normal saline for cell viability counting. The RPMI-1640 medium was enriched with 10% heat-inactivated FBS (heated at 56°C for 30 minutes), 100 units/ml penicillin, and 2 mg/ml streptomycin before use. Trypsin (0.25×10^{-1}% w/v) was used for cell harvesting, while a 1% v/v acetic acid solution was utilized to dissolve unbound SRB dye. SRB (0.40%) dissolved in a 1% acetic acid solution served as a protein dye. A concentrated solution of trichloroacetic acid (50%) was formulated and preserved for future use. It was used by adding 50 µL of the stock solution to 200 µL of RPMI-1640 medium per well, resulting in a final protein precipitation concentration of 10%. Additionally, 100% isopropanol and 70% ethanol were employed. To facilitate the solubilization of SRB dye, a 10 mM Tris base solution at pH 10.50 was prepared by dissolving 121.10 g of Tris base in 1000 ml of distilled water and adjusting the pH using (2 M) HCl.

2.1.5. Instrumentation

Elemental composition analysis involving carbon, hydrogen, and nitrogen was performed at the Microanalytical Center of Cairo University in Egypt. This analysis utilized a CHNS-932 (LECO) Vario elemental analyzer. To determine the melting points of the samples, a triforce XMTD-3000 instrument was employed. Metal content analyses were conducted at the Egyptian Petroleum Research Institute using inductively coupled plasma atomic absorption spectrometry (ICP). Fourier-transform infrared spectroscopy (FT-IR) analyses, spanning from 4000 to 400 cm^{-1}, were recorded using KBr disks and a Perkin-Elmer 1650 spectrometer. The Jenway 4010 conductivity meter was utilized to determine the molar conductivities of 10^{-3} M solutions of the solid complexes in DMF. Mass spectra were acquired through the electron ionization method at 70 eV using an MS-5988 GS-MS Hewlett-Packard instrument at the Microanalytical Center of Cairo University. Thermal analyses, such as thermogravimetric (TG) and differential thermogravimetric (DTG) measurements of both the Schiff base ligand and metal complexes were conducted employing a Shimadzu TG-50H thermal analyzer, covering a temperature range from ambient conditions to 1000

°C.Spectrophotometric measurements in solution were carried out utilizing an automated UV–Vis spectrophotometer, specifically the PerkinElmer Model Lambda 20, spanning a wavelength range from 200 to 700 nm. Anticancer efficacy tryouts were conducted at the Institute of National Cancer, specifically within the Cancer Biology and Pharmacology Departments at Cairo University, Egypt. Antimicrobial assessments were performed at Cairo University's Microanalytical Center, while anti-*H. Pylori* activity assessments were conducted at the Microanalytical Center at Cairo University.

2.2. Preparation of Schiff base ligand

A novel Schiff base ligand referred to as (**L_1**) was synthesized using a proposed method involving the condensation of 4-hydrazineylquinazoline (4.370 mmol, 0.7 g) and (E)-1-(2-(p-tolyl)hydrazineylidene)propan-2-one (4.370 mmol, 0.770 g) in hot 100% ethanol at 60°C. The mixture of this reaction underwent reflux for a duration of 4 hours. Following the evaporation of the DMF-ethanol mixture, filtration, and recrystallization, an orange solid of the resulting pure Schiff base was obtained with a yield of 96%. Scheme (1) depicts the structure of (**L_1**) and the reaction leading to its formation. The pure Schiff base (**L_1**) obtained had a yield of 96% and appeared as an orange solid with a melting point of 210°C. Analytically, the calculated composition for **$C_{19}H_{19}N_5$** (%): Carbon (C) comprises 71.90%, Hydrogen (H) constitutes 6.03%, and Nitrogen (N) constitutes 22.07%. Experimentally found composition (%): C, 71.53; H, 5.88; N, 21.82. The infrared (IR) spectrum displayed characteristic peaks at 3437sh (NH), 1605sh (C = N), and 1545sh (υ(C=N) Pyridine). The ultraviolet-visible (UV-vis) spectrum showed absorption peaks at λmax, nm: 314 (π–π*), 334 (n–π*), and 388 (charge transfer).

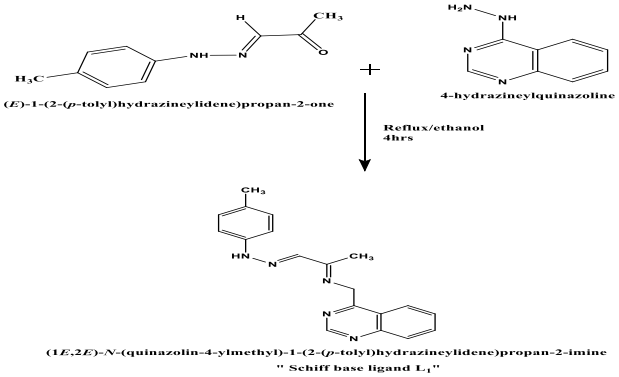

Scheme. 1. Synthesis pathway of (**L_1**).

2.3. Preparation of ternary complexes.

A standardized procedure was utilized to create mixed ligand complexes, employing specially prepared Schiff base ligands denoted as (**L_1**) as the main ligands. The **L_1** Schiff base ligands (0.314 mmol, 0.1 g) were solubilized in 40 ml of hot absolute ethanol. In a separate solution, the secondary ligand, the amino acid Methionine (0.314 mmol, 0.046 g), was solubilized in 10 ml of hot distilled water. The chelates were created by combining a hot solution of the primary Schiff base ligand (**L_1**) in absolute ethanol with the secondary ligand methionine in distilled water. Following this, a hot ethanoic solution (20 ml) containing the relevant metal chloride salt (such as $MnCl_2.4H_2O$, $CoCl_2$ $.6H_2O$, $CdCl_2.2H_2O$) (0.314 mmol) was gradually added drop by drop to the mixture. The resultant solution underwent reflux for a duration of 4 hours, resulting in the formation of precipitates that represented the complexes. These precipitates were gathered via filtration and underwent further purification through multiple washes using a combination of ethanol and water. Subsequently, they were dried under vacuum conditions using anhydrous $CaCl_2$.

2.3.1. [(L1) (L2) Mn (Cl)].2H2O

A brown solid compound was synthesized with a yield of 95%. Its melting point is 298°C. Elemental analysis indicates the theoretical composition **(C_{23} H_{32} Mn Cl N_7 O_4 S)** should contain C (46.58%), H (5.39%), N (16.53%), O (10.79%), S (5.40%), Cl (5.97%), and Mn (9.26%). The actual found composition shows C (46.41%), H (5.22%), N (16.43%), O (10.66%), S (5.28%), Cl (5.86%), and Cd (9.15%). Physical characterization includes conductivity (Λm) of 23 Ω^{-1} mol^{-1} cm^2. The compound's FT-IR spectrum displays absorption peaks at 1631 cm^{-1} (sh, two azomethine C=N stretches), 1571 cm^{-1} (m, azomethine C=N in Pyridine), 1421 cm^{-1} (m, asymmetric ν (COO)), 1355 cm−1 (s, symmetric ν (COO)), 595 cm^{-1} (w, metal-oxygen bond), and 475 cm^{-1} (w, metal-nitrogen bond). In terms of UV-Vis spectroscopy, the compound exhibits absorbance peaks at 306 nm (associated with π–π* transitions), 339 nm (related to n-π* transitions), and 409 nm (indicative of charge transfer).

2.3.2. [(L1) (L2) Co (Cl)].3H2O

A dark brown solid compound was obtained with a yield of 97% and a melting point of 315°C. The elemental analysis yielded the following results: Calculated for **(C_{23} H_{34} Co Cl N_7 O_5 S)** - C: 44.91%, H: 5.57%, N: 15.94%, O: 13%, S: 5.21%, Cl: 5.76%, Co: 9.58%. The actual values found were: C: 44.81%, H: 5.44%, N: 15.77%, O: 12.88%, S: 5.21%, Cl: 5.62%, Co: 9.41%. The compound displayed a molar absorptivity of 17 Λm (Ω^{-1} mol^{-1} cm^2). Its FT-IR spectrum showed characteristic peaks at 1629 cm^{-1} for two azomethine (C=N) groups, a peak at 1565 cm^{-1} for azomethine (C=N) in Pyridine, and peaks at 1426 cm^{-1} and 1340 cm^{-1} for asymmetric and symmetric

vibrations of (COO) groups respectively. Additionally, the spectrum displayed peaks at 565 cm^{-1} and 476 cm^{-1} corresponding to (M─O) and (M─N) vibrations, respectively. In the UV–Vis spectrum, the compound exhibited peaks at 290 nm, 294 nm, and 296 nm, indicating π–π* conjugated systems, while a peak at 334 nm indicated n-π* transitions. Furthermore, a peak at 357 nm indicated a charge transfer.

2.3.3. [(L1) (L2) Cd (Cl)]

A dark brown solid was obtained in 98% yield with a melting point of 296°C. The elemental analysis (C, H, N, O, S, Cl, Cd) was calculated and compared against the found values for a compound with the formula **(C_{23} H_{28} Cd Cl N_7 O_2 S)**. The comparison showed close alignment between the calculated and found percentages, affirming the synthesis. Additionally, spectroscopic data was gathered: the molar conductivity (Λm) was measured as 19 Ω^{-1} mol^{-1} cm^2. The compound displayed distinctive peaks in the Fourier-transform infrared spectroscopy (FT-IR) spectrum at specific wavenumbers: two peaks for azomethine (C=N) at 1616 (shoulder) and 1567 (medium), asymmetric ν (COO) at 1418 (medium), symmetric ν (COO) at 1352(strong), as well as metal-oxygen (M─O) at 590 (weak) and metal-nitrogen (M─N) at 466 (weak) stretching vibrations. In the UV-Vis spectrum, characteristic peaks were observed at wavelengths 312 nm (π–π*), 294 and 331 nm (n- π*), and a charge transfer peak at 379 nm. These spectral characteristics offer insights into the compound's structure and electronic transitions.

2.4. Spectrophotometric studies

Absorption spectra were obtained for solutions containing the unbound Schiff base ligand **(L_1)** and its corresponding metal complexes at a concentration of 1 X 10^{-4} M. These spectra were measured by scanning across a range of wavelengths from 200 to 700 nm.

2.5. Computational methodology

The Schiff base ligand **(L_1)** and its metal complexes underwent theoretical computations using the software package of Gaussian 09w. Density Functional Theory (DFT) was chosen as the computational method for these analyses. The molecular configuration structure of the tested compounds was extensively optimized by employing the B3LYP method combined with the LANL2DZ basis set for both the Schiff base ligand **(L_1)** and its metal complexes [19]. Visualization of the optimized structure of the ternary complex was carried out using version 1.8 package of Chemcraft and version 6.0.16. of GaussView. Crucial parameters of chemical quantum such as the energies of the Highest Occupied Molecular Orbital (E_{HOMO}) and the Lowest Unoccupied Molecular Orbital (E_{LUMO}) were computed, alongside the HOMO–LUMO energy gap (ΔE) for the molecule under study. These parameters offer essential visions on the electronicstructure and reactivity of the ligand.

2.6. Antimicrobial activity

The investigation focused on evaluating the antimicrobial potential of the substances through the agar well diffusion technique. The study encompassed in vitro assessments targeting both Gram(+ve) bacteria, namely *Staphylococcus aureus* and *Streptococcus mutans*, and Gram(-ve) bacteria for instance *Pseudomonas aeruginosa*, *Escherichia coli*, and *Klebsiella pneumonia*. These examinations were carried out using a nutrient agar medium. Additionally, the compounds were tested for their antifungal properties against Candida albicans and *Aspergillus niger*, utilizing Sabouraud dextrose agar medium. For comparative purposes, standard medications such as Gentamicin and Ampicillin were used against Gram(-ve) and Gram(+ve) bacteria, respectively, while Nystatin was employed for fungal strains. To maintain consistency, DMSO functioned as the solvent control. This compounds were assessed at a concentration of 15 milligrams per milliliter against bacterial and fungal strains in the experimentation.

2.6.1. Method of testing

The process began by pouring sterilized media, approximately 20-25 mL in each Petri dish, which was then allowed to undergo solidification at ambient temperature. To create a microbial suspension corresponding to the McFarland 0.5 standard solution (1.5x 10^5 CFU mL^{-1}), sterile saline was used. The turbidity of the solution was modulated to an optical density (OD) of 0.13 utilizing a spectrophotometer configured at a wavelength of 625 nm [20]. Once the suspension's turbidity was adjusted, a sterile cotton swab was dipped into the prepared solution and spread across the dried agar surface. Afterward, the swab was left to dry for 15 minutes with the lid on. Using aseptic borers, perforations with a diameter of 6 mm were generated in the solidified substrate [21]. Subsequently, a volume of 100 μL of the test compound solution was meticulously introduced into each well by means of a micropipette. The agar-filled receptacles were subsequently transferred to an incubation chamber maintained at a temperature of 37°C for a duration of 24 hours, facilitating the examination of potential antibacterial effects. This experimental procedure was approved out in triplicate, and the zones of inhibition were measured in millimeters [21].

2.7. Anti-H. Pylori activity

The assessment of the effectiveness of Schiff base **(L_1)** and its metal complexes against H. pylori ATCC 43504, sourced from the American Type Culture Collection, involved employing the micro-dilution

broth method. The determination of the minimal inhibitory concentration (MIC) and minimal bactericidal concentration (MBC) of these compounds was carried out using Mueller-Hinton broth supplemented with lysed horse blood [22].

2.7.1. Minimal inhibitory concentration (MIC)

The MIC (minimal inhibitory concentration) of the test extracts was assessed using the micro-dilution broth technique. This method involved using Mueller-Hinton broth enriched with lysed horse blood. The concentration range of the test extracts was established through serial two-fold dilutions, spanning from 0.98 to 1000 µg/mL. For the experiment, sterile 96-well polystyrene microtitrate plates were employed. Each well contained 200 µl of the respective extract dilution within the broth medium. Inocula were prepared from fresh microbial cultures in sterile 0.85% NaCl, adjusted to a turbidity equivalent to the 1.0 McFarland standard. 2 µl of this inoculum were introduced into each well to reach a final density of 3.0×10^6 CFU (colony forming units)/ml. The incubation period lasted 72 hours at 35°C in a microaerophilic environment with 15% CO_2. Following this incubation, the MICs were determined by visually identifying the lowest concentration of the extract that completely inhibited the growth of the reference strain. Each microplate included a positive control (containing only the inoculum without the test extracts) and a negative control (containing the test extracts without any inoculum) [22].

2.7.2. Minimal bactericidal concentration (MBC)

The Minimum Bactericidal Concentration (MBC) was determined by transferring 100 ml of the microbial culture from wells where complete growth inhibition was observed, including the last positive well and the growth control well, onto Mueller-Hinton agar plates that contained 5% horse blood. These plates were subsequently placed in an incubator at 35°C for a period of 72 hours under microaerophilic conditions. The MBC was defined as the lowest concentration of the tested extracts at which no microbial growth was detected. In order to determine whether the tested extracts exhibited bactericidal or bacteriostatic effects, we calculated the MBC/MIC ratios. It's worth noting that, in this study, antibacterial agents were considered bactericidal if the MBC/MIC ratio was no more than four times the MIC value [20]. Each experiment was performed in triplicate, and the results presented in this report are representative of the overall findings.

2.8. Anticancer activity

In order to assess the potential cytotoxicity of both the Schiff base ligand and its corresponding metal complexes, the study utilized a method developed by Skehan and Storeng [23]. The experiment involved the use of a 96-well plate with 104 cells in each well, allowing a 24-hour period for cell adhesion to the well's surface. The compounds being examined, including the Schiff base ligand and its metal complexes, were scanned at various concentrations (12.5 µg ml^{-1}, 25 µg ml^{-1}, 50 µg ml^{-1}, and 100 µg ml^{-1}), with each concentration evaluated in triplicate. Following the introduction of the test compounds, the cell monolayer was incubated for 48 hours at 37°C in an environment with 5% CO_2. After this incubation period, the cells underwent fixing, washing, and staining using SRB stain. Excess stain was removed with acetic acid, and by using tris–EDTA buffer the remaining stain was eluted. The optical density (O.D.) of individual wells was assessed at a wavelength of 564 nm using a spectrophotometer, with automatic subtraction of the mean background absorbance. Mean values for each concentration of the tested compounds were then calculated. To evaluate the compounds' impact on cell survival, a correlation was established between the surviving fraction and the drug concentration, creating a survival curve for the specific breast tumor cell line that was the focus of the study.

The study aimed to determine the survival rate of cells by applying the next formula:

Survival fraction = Optical Density (O.D.) of treated cells / Optical Density (O.D.) of control cells.

The basic objective of this exploration was to compute the IC_{50} values. These values represent the concentrations of either the Schiff base ligand or its metal complexes necessitated to reduce cell growth by 50%. The entire research was carefully conducted three times for the MCF7 cell line to ensure the consistency and reliability of the results. In brief, this study employed a well-established methodology to assess the potential cytotoxic effects of the Schiff base ligand and its metal complexes. It utilized a range of concentrations and various analytical techniques to evaluate their impact on the growth of breast tumor cells. The IC_{50} values were determined to assess the effectiveness of these compounds in inhibiting cell growth, and the experiment was rigorously replicated to enhance the scientific reliability of the findings.

2.9. Molecular docking

Molecular docking studies utilized MOE 2014 software, known for its adeptness in rigid molecular docking, to predict potential binding modes of both the Schiff base ligand **(L_1)** and its Cd (II) complex with significant receptors. The investigation targeted crystal structures of essential receptors, including (PDB ID: **3AHU, 1GHP, 2ZIC, 4N74, 5JPE**), in

addition to microtubules, crucial elements of the breast cancer receptor mutant oxidoreductase (PDB ID: **3HB5**), and the crystal structure of the SARS-CoV-2 receptor binding domain bound to the human antibody CR3022 (PDB ID: **6W41**). The software facilitated the computation and presentation of potential docking configurations of the receptors with the Schiff base ligand and its complex molecules. For the input files, exclusion of extraneous components such as water molecules, co-crystallized ligands, and unsupported elements like Na, K, Hg, etc., was done. However, amino acid chains were retained for further analysis [24]. Using Gaussian software, the Schiff base ligand **(L_1)** and its Cd (II) complex were generated in PDB file format. Crystal structures of all receptors were sourced from the Protein Data Bank (PDB) available at http://www.rcsb.org/pdb. This methodology facilitated the exploration of potential binding interactions and assessment of the interaction between the Schiff base ligand **(L_1)** and its Cd (II) complex with these vital receptors. The resulting analysis provided valuable insights into potential therapeutic applications.

3. Findings and Analysis

3.1. Characterization of the Schiff base (L1)

The elemental analysis conducted on the tridentate Schiff base ligand **(L_1)** confirmed that the empirical data matched the calculated values, validating its molecular formula as **$C_{18}H_{18}N_6$**. This compound displayed favorable physical attributes, including a melting point around 210°C and demonstrated solubility in various solvents like ethanol, DMF, and DMSO, exhibiting an orange hue. The ^{1}H NMR spectrum of the Schiff base ligand revealed the presence of a proton in the NH group at 10.46 and 11.61 ppm, as well as azomethine protons at 7.94 ppm and aromatic protons ranging from 7.45 to 8.13 ppm, as detailed in Table 3. The absence of any indications of the NH_2 group serves as confirmation for the successful synthesis of Schiff base ligand (L_1). In the experimental UV-Vis absorption spectrum, three distinct bands were observed for the Schiff base ligand. These bands appeared at 314 nm, indicating π-π* transitions, 334 nm, corresponding to n-π* transitions, and 388 nm, which was associated with charge transfer processes. Moreover, the structural characteristics of the Schiff base ligand **(L_1)** were further elucidated through mass spectrum analysis. The recorded spectrum revealed a molecular ion peak at m/z = 318.78 atomic units, which aligns with the expected molecular weight for the ligand with a formula of **$C_{18}H_{18}N$**, calculated to be 318.38 g/mol. The IR spectrum of the prepared Schiff base ligand **(L_1)** revealed significant bands that correlated with the structure of the ligand. Specifically, a distinct band at 1605 cm^{-1} indicated the presence of two azomethine groups, while the band at 1545 cm^{-1} corresponded to (C=N) Pyridine. Moreover, a sharp vibration band attributed to ν (N–H) was identified at 3437 cm^{-1}, in accordance with values listed in Table 1 [25]. The theoretical frequencies obtained through DFT were recorded at 3580, 1655, and 1590 cm^{-1}, showing a close alignment with the experimental data. This alignment strongly supported the effective formation of the Schiff base ligand **(L_1)** and validated the proposed chemical structure, as depicted in Figure 1. Discrepancies between the theoretical and experimental frequencies might be due to systematic errors arising from factors such as harmonicity or the use of gas phase molecules in the DFT calculations. To mitigate these errors, a correlation coefficient of 0.9648 was applied for LAN2DZ [26, 27]. This analysis provided valuable insights into the structure of the Schiff base ligand **L_1**, as depicted in Figure 2.

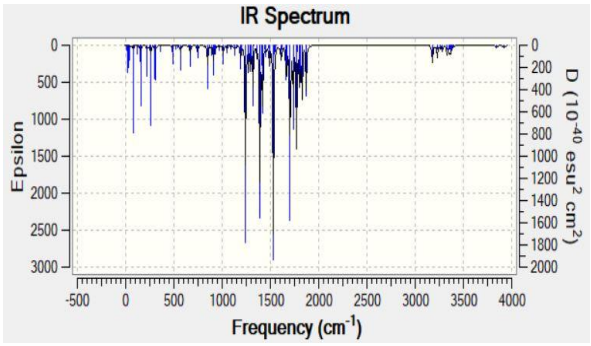

(A)

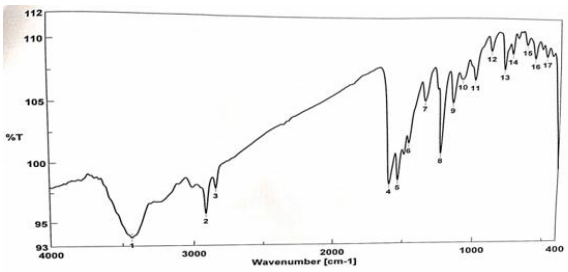

(B)

FIGURE 1. IR spectra of Schiff base ligand **(L_1)** (A) theoretical spectrum and (B) experimental spectrum.

FIGURE. 2. The optimized structure of Schiff base ligand (**L_1**)

3.2. Characterization of Schiff base metal complexes.

3.2.1. Elemental analysis

Three distinct transition metal complexes were synthesized by combining equal amounts of a Schiff base **(L_1)** and Methionine ligand with Mn (II), Co (II)

and Cd (II) metal salts in appropriate solvents. Thorough elemental analyses were carried out, examining molecular formulas, melting points, and various physical properties of these compounds. Remarkably, these complexes exhibited stability at room temperature and displayed high melting points. Notably, they were insoluble in water and ethanol but exhibited high solubility in DMF and DMSO solvents. Both estimated values and experimental elemental analyses showed a significant level of correlation. According to the data presented in Table 1, the complexes prominently displayed a 1:1:1 ratio, wherein each metal ion formed a bond with one Schiff base **(L_1)** ligand and one Methionine ligand. Consequently, this resulted in a complex with a stoichiometry represented as **M: L_1: L_2**.

Table. 1. Presentation of Physical and Analytical Data for L_1 and Corresponding Metal Complexes.

Compound (chemical formula)	Color Yield (%)	M.p. (°C)	Found (Calcd)						A_m (Ω^{-1} mol^{-1} cm^2)
			C(%)	H(%)	N(%)	S(%)	Cl (%)	M (%)	
Schiff base ligand (L_1) $C_{19}H_{19}N_5$	Orange (96)	210	71.53 (71.90)	5.88 (6.03)	21.82 (22.07)	……	……	……	……..
(3) [(L_1) (L_2) Mn(Cl)].2H_2O ($C_{23}H_{32}$Mn Cl N_7O_4 S)	Brown (95)	298	46.41 (46.58)	5.22 (5.39)	16.43 (16.53)	5.28 (5.40)	5.86 (5.97)	9.15 (9.26)	23
(1) [(L_1) (L_2) Co (Cl)].3H_2O ($C_{23}H_{34}$Co Cl N_7O_5 S)	dark brown (97)	315	44.81 (44.91)	5.44 (5.57)	15.77 (15.94)	5.15 (5.21)	5.62 (5.76)	9.41 (9.58)	17
(2) [(L_1) (L_2) Cd (Cl)] ($C_{23}H_{28}$Cd Cl N_7O_2 S)	dark brown (98)	296	44.84 (44.91)	4.42 (4.55)	15.81 (15.96)	5.13 (5.20)	5.70 (5.76)	18.17 (18.29)	19

3.2.2. Molar conductivity measurements

The assessment of conductivity is employed to determine the extent of ionization within metal complexes. To analyze the molar conductivity of Schiff base ligand **(L_1)** metal complexes, investigations were conducted in different solvents selected for their compound solubility. These assessments used a concentration of 1.0×10^{-3} M at a temperature of 25°C. The results notably showed that all Schiff base ligand **(L_1)** metal complexes exhibited behavior characteristic of non-electrolytes because no counter ions are present outside coordination sphere of mixed ligand complexes, as outlined in Table 2 [28, 29, 30].

Table 2: EI- mass data of L_1 Schiff base metal complexes.

Compound	m/z value		Interpretation
	Calculated	Found	
Schiff base ligand (L_1)	318.38	318.78	$[M+1]^+$
Methionine (L_2)	149.211	149	$[M]^+$
(1) [(L_1) (L_2) Mn (Cl)].2H_2O	593	592	$[M]^+$
(2) [(L_1) (L_2) Co (Cl)].3H_2O	615.02	616	$[M+1]^+$
(3) [(L_1) (L_2) Cd (Cl)]	614.45	614	$[M]^+$

3.2.3. Spectrophotometric Analysis of L1 and its Metal Coordination Compounds in the UV–Visible Range

The investigation of the electronic spectra of the tridentate Schiff base ligand **(L_1)** and its metal complexes was carried out, examining wavelengths between 200 and 700 nm in a suitable solvent. When analyzing the UV-Vis spectrum of the isolated Schiff base ligand, distinct absorption bands were identified at 314, 334, and 388 nm. These absorptions were linked to specific transitions: the 314 nm band was associated with π-π* transitions, the 334 nm band represented n-π* transitions occurring within the -C=N- group, and the higher-energy band at 388 nm was attributed to charge transfer [31, 32]. Upon coordination with various metal ions, noticeable shifts were observed in the bands of the Schiff base ligand **(L_1)** spectrum. The band at 314 nm in the ligand spectrum shifted to lower wavelengths, ranging between 290 and 312 nm in all complexes. This shift indicated alterations in the π-π* transitions. Moreover, the band related to the azomethine group, initially observed at 334 nm in the ligand spectrum, showed a shift to the range of 345–371 nm in the complexes, suggesting changes in the n-π* transitions [34]. This spectral data strongly implies the contribution of the azomethine (C=N) group nitrogen in coordination with the metal ions.

3.2.4. ^{1}H-NMR spectral studies

The proposed bonding pattern in the synthesized complexes is substantiated by the analysis of ^{1}H-NMR spectra. The recorded ^{1}H-NMR spectra of the synthesized Schiff base ligand **(L_1)** and its Cd(II) complex were conducted in DMSO-d6, with measurements of their respective chemical shift values (ppm). In the ligand spectrum, multiplet signals at 7.45-7.49 ppm were identified, corresponding to the aromatic phenol group, while signals at 8.04-8.22 ppm were assigned to the aromatic phenol group of pyridine, as outlined in Table. These signals were also evident in the Cd(II) complex, appearing at 7.45-7.53 ppm and 7.94-8.491 ppm, respectively. Moreover, the proton signals from the NH group manifested as singlets at 11.13 and 9.68 ppm in the Schiff base ligand **(L_1)**. These signals persisted in the Cd (II) complex but underwent a shift to higher values, registering at 11.531 and 10.078 ppm, respectively. Additionally, the proton signals from the N-CH=N in pyridine were observed as singlets at 8.49 ppm in the Schiff base ligand **(L_1)**. In the Cd(II) complex, these signals remained detectable but shifted to a lower value at 7.874 ppm, indicating the chelation effect, as outlined in Table 3. The protons from the methyl group (attached to the sulfur atom) and the amino groups of the amino acid Methionine were observed at 2.09 and 1.35 ppm, respectively. This observation suggests that chelation occurred in the Cd (II) complex through the binding of Cd to the amino group of methionine.

Table 3: The ^{1}H NMR spectral Analysis for **L_1** and its Cd (II) metal complex: Comparative Spectral Data

Compound	Chemical shift, (δ) ppm	Assignment
Schiff base ligand (L_1)	**11.13**	**(s, H, ph-NH)**
	9.684	**(s, H, NH-Pyridine)**
	7.97	**(s, H, N=CH)**
	7.45-7.49	**(m, 8H, aromatic)**
	8.04-8.22	**(m, 4H ,pyridine)**
	8.49	**(S, H, N-CH=N)**
	2.07	**(s, 3H, N=C-CH_3)**
	2.32	**(s, 3H, ph-CH_3)**
[(L_1)(L_2)Cd Cl]	**11.531**	**(s, H, ph-NH)**
	10.078	**(s, H, NH-Pyridine)**
	7.874	**(s, H, N=CH)**
	7.45-7.53	**(m, 4H, aromatic)**
	7.94-8.491	**(m, 4H ,pyridine)**
	8.31	**(S, H, N-CH=N)**
	2.07	**(s, 3H, N=C-CH_3)**
	2.32	**(s, 3H, ph-CH_3)**
	1.75	**(s, 2H, CH-NH_2)**
	3.410	**(s, 2H, NH_2-CH-C=O)**
	2.041	**(q, 2H, CH2-CH2-CH**
	2,720	**(t, 2H, S-CH2-CH2)**
	2.109	**(s, 3H, CH3-S)**

3.2.5. Thermal analysis of ternary Schiff base metal complexes

The research employed Thermal Gravimetric

Analysis (TGA) to assess the thermal stability of newly synthesized metal complexes and differentiate between water molecules existing in hydrated or coordinated states within their structures [33, 34, 35, and 36]. The TG and DTG analysis were conducted on Schiff base ligand metal complexes, investigating their behavior across a wide temperature range from room temperature up to 1000°C. The findings included details regarding temperature ranges, stages of decomposition, percentage of product loss during decomposition, calculated versus observed weight loss percentages, and residues of all compounds, as outlined in Table 4. Distinct decomposition steps were observed in the thermal analysis of several complexes—namely **[(L_1) (L_2) Mn (Cl)].2H_2O, [(L_1) (L_2) Co (Cl)].3H_2O,** and **[(L_1) (L_2) Cd (Cl)].** The thermal analysis of the **[(L_1) (L_2) Mn (Cl)].2H_2O** complex, with the chemical formula **(C_{23} H_{32} Mn Cl N_7 O_4 S),** displayed four decomposition steps. The initial step, between 50-135°C with a peak at 90°C, led to the loss of two hydrated water molecules, estimating a mass loss of 6.35% (calculated = 6.70%). The subsequent step, between 135-230°C with a peak at 210°C, involved the loss of **C_4 H_{10} Cl S** with an estimated mass loss of 20.89% (calculated = 21.18%). The final third step, between 230-800°C with a peak at 485°C, indicated the loss of **C_{19} H_{18} N_7 O** with an estimated mass loss of 60.70% (calculated = 60.79%). After complete decomposition, magnesium oxide **(MnO)** remained as residues.

In the case of the **[(L_1) (L_2) Co (Cl)].3H_2O** complex, characterized by the chemical formula **(C_{23} H_{34}Co Cl N_7 O_5 S),** the first decomposition step took place within the range of 35-110°C, with a peak observed at 80°C, signifying the loss of three hydrated water molecules.

This accounted for an estimated mass loss of 8.63% (calculated = 8.70%). The subsequent step occurred from 110-545°C with a peak at 270°C, involving the loss of **C_{13} H_{21} Cl N_2 O S,** resulting in an approximated mass loss of 47.50% (calculated = 47.50%). The final step, spanning 545-800°C with a peak at 575°C, indicated the loss of **$C_{10}H_7N_5$,** leading to an estimated mass loss of 31.70% (calculated = 32.07%). This left behind cobalt oxide **(CoO)** as the decomposition product.

For the **[(L_1) (L_2) Cd (Cl)]** complex with the chemical formula **(C_{23} H_{28} Cd Cl N_7 O_2 S),** the initial decomposition occurred between 40-215°C, peaking at 95°C, resulting in the loss of **C_6 H_{13} N O S,** with an approximated mass loss of 23.80% (calculated = 24.01%). The subsequent step took place between 215-800°C with a peak at 335°C, indicating the loss of **C_{17} H_{15} Cl N_6,** resulting in an estimated mass loss of 55.34% (calculated = 55.53%), leaving behind Cadmium oxide (**CdO)** as the product of decomposition.

Table 4: Thermoanalytical results (TG and DTG) of Schiff base ligand (**(L_1)**) and its metal complexes.

Complex	TG-range (oC)	DTG max	n *	Mass loss Estim (calcd)% (Total mass Loss)	Assignment	Residues
(1) **[(L_1) (L_2) Mn (Cl)].2H_2O** **(C_{23} H_{32} Mn Cl N_7 O_4 S)**	**(50-135)** **(135-230)** **(230-800)**	**90** **210** **485**	**1** **2** **3**	**6.35(6.70)** **20.89(21.18)** **60.70(60.79)**	**-Loss of 2H_2O** **-Loss of C_4 H_{10} Cl S** **-Loss of C_{19} H_{18} N_7 O**	**MnO**
(2) **[(L_1) (L_2) Co (Cl)].3H_2O** **(C_{23} H_{34}Co Cl N_7 O_5 S)**	**(34-110)** **(110-545)** **(545-800)**	**80** **270** **575**	**1** **2** **3**	**8.63(8.70)** **47.50(47.59)** **31.7(32.07)**	**-Loss of 3H_2O** **-Loss of C_{13} H_{21} Cl N_2 O S** **-Loss of C_{10} H_7 N_5**	**CoO**
(3) **[(L_1) (L_2) Cd (Cl)]** **(C_{23} H_{28} Cd Cl N_7 O_2 S)**	**(40-215)** **(215-800)**	**95** **335**	**1** **2**	**23.80(24.01)** **55.34(55.53)**	**-Loss of C_6 H_{13} N O S** **-Loss of C_{17} H_{15} Cl N_6**	**CdO**

3.2.6. IR spectra

To deduce the binding mode of **(L_1)** with metal (II) ions, an analysis compared the IR spectra of the free **(L_1)** ligand and Methionine ligand with those of the resultant metal complexes [37]. In the IR spectrum of the Schiff base ligand, six prominent peaks were noted, with the most significant at 1605 and 1545 cm^{-1}, attributed to the (C=N) azomethine and (C=N) pyridine, respectively. In the metal complexes, these peaks shifted to higher wavenumbers: 1629, 1565 cm^{-1} for Co (II), 1616, 1567 cm^{-1} for Cd (II), and 1631, 1571 cm^{-1} for Mn(II). This alteration strongly implies

the involvement of (C=N) groups in coordination [38]. Moreover, a broad vibration band associated with the ν (N–H) was observed within the 3430-3437 cm^{-1} range, indicating the stretching vibration of the coordinated water molecule's N-H bonds. In the complex spectra, the characteristic band υ (CH_2-S) of methionine remains unaltered. Two other characteristic bands were observed at 1426, 1340 cm^{-1} for Co(II), 1418, 1421, 1355 cm^{-1} for Mn(II) and 1352 cm^{-1} for Cd(II) linked to (COO^-) asy and (COO^-) sym, indicating the Methionine ligand's carboxylic group's involvement in coordination with the metal ions (Table 3) [39, 40 ,41]. Furthermore, distinctive new bands appeared in all metal complex spectra between 565–595 cm^{-1} and 466–476 cm^{-1}, suggesting the establishment of M-O and M-N bonds, respectively (Table 5) [42]. The spectral features discussed serve as illustrative instances in theoretical investigations, with a specific emphasis on the application of Density Functional Theory (DFT), as illustrated in Figure 3 for cadmium complex as an example. The recorded frequencies align notably with the theoretical predictions, confirming the successful synthesis of mixed ligand complexes involving a Schiff base ligand **(L_1)**. The agreement between experimental and theoretical frequencies supports the proposed chemical structure of the mixed ligand complex. Discrepancies observed between theoretical and experimental frequencies may be attributed to systematic errors, potentially stemming from harmonicity or the use of gas-phase molecules in DFT calculations. To address these disparities, a correlation coefficient of 0.9648 was applied for LAN2DZ, serving as a corrective measure to improve the accuracy of theoretical predictions and reduce the impact of systematic errors [43, 44]. These observations propose that the Schiff base ligand **(L_1)** functioned as a neutral tridentate ligand, coordinating to metal ions via two N-azomethine and (C=N) pyridine. Simultaneously, by comparison with similar compounds (Gupta and Srivastava, 1985), the metal coordinated to the Methionine moiety using NH_2 and COO^- groups, forming a uninegative bidual ligand [45, 46].

Table 5. Key Infrared (IR) Spectral Bands of Isolated Schiff base ligand **(L_1)** and their Ternary Complexes: Key Wavelength Ranges

Compound	υ (CH_2-S)	υ(C=N)	υ(C=N) Pyridine	υ(COO) Asymmetric	υ(COO) symmetric	υ(M-O)	υ(M-N)
Schiff base ligand(L_1)	**2916sh**	**1605**	**1545**	-	-	-	-
(1) [(L_1) (L_2) Mn (Cl)].2H_2O	**2917sh**	**1631sh**	**1571m**	**1421m**	**1355s**	**595w**	**475w**
(2) [(L_1) (L_2) Co (Cl)].3H_2O	**2918sh**	**1629sh**	**1565m**	**1426m**	**1340s**	**565w**	**476w**
(3) [(L_1) (L_2) Cd (Cl)]	**2918sh**	**1616sh**	**1567m**	**1418m**	**1352s**	**590w**	**466w**

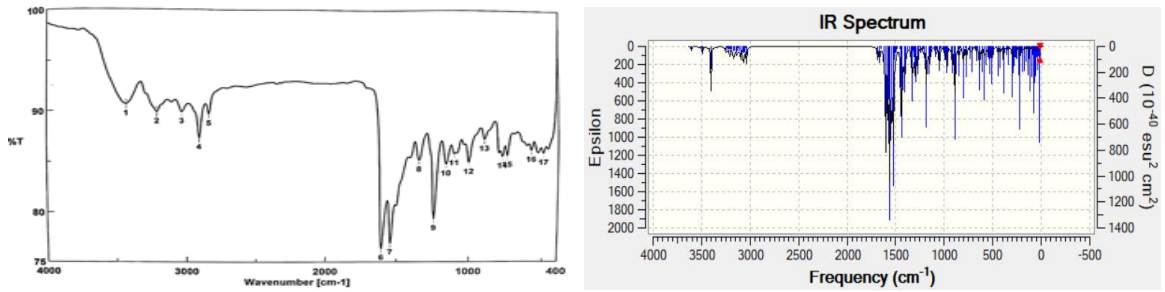

(A) (B)

FIGURE .3. IR spectra of Schiff base ligand **(L_1)** cadmium (II) complex **[(L_1) (L_2) Cd (Cl)]** (A) experimental spectrum and (B) theoretical spectrum.

3.2.7. Structural interpretation

The structural analysis of ternary complexes formed by the tridentate Schiff base ligand **(L_1)** in conjunction with Methionine ligands and Co(II), Cd(II), and Mn(II) was conducted through multiple analytical techniques. These methods encompassed elemental analyses, molar conductance measurements, as well as IR, UV-Vis, mass, and thermal analyses. Utilizing the collected data, proposed structures for the transition metal complexes were formulated and illustrated in Scheme 2.

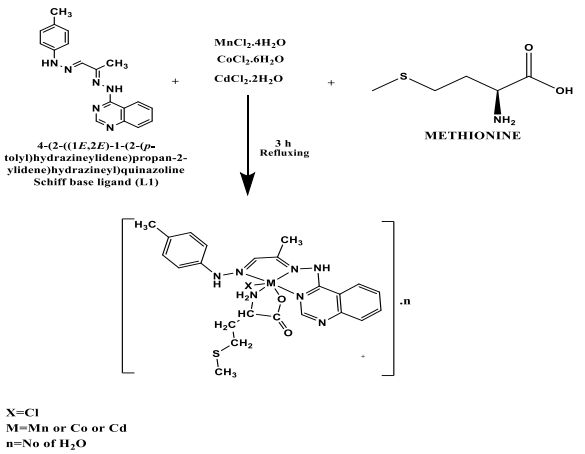

Scheme. 2. Suggested structure of ternary complex for example

3.3. Geometry optimization

The molecular structures of **L₁** and its Cd (II) complex were optimized through geometry optimization occupying Density Functional Theory (DFT), and their atomic numbering is visually represented in Figure 4 [47]. Specifically, the fully optimized geometries reveal a distorted octahedral coordination sphere surrounding the Cd (II) ion, as indicated by the values of chosen bond lengths and angles calculated for the Cd(II) complex, detailed in Table 6 [48]. These computations revealed a slight elongation in specific bond lengths, such as N(8)-N(9), N(12)-N(13), and N(15)-C(16) within the Cd(II) complex, suggesting coordination of the ligand **(L₁)** through two azomethine nitrogen and the azomethine group of pyridine. Furthermore, critical molecular orbitals influencing chemical stability—namely, the HOMO (highest occupied molecular orbital) and LUMO (lowest unoccupied molecular orbital)—were identified. The HOMO typically acts as an electron donor, whereas the LUMO functions as an electron acceptor. Additional important parameters, including the HOMO–LUMO energy gap (ΔE), absolute electronegativities (χ), chemical potentials (Π), absolute hardness (η), absolute softness (σ), global electrophilicity (ω), global softness (S), and additional electronic charge (ΔNmax), were computed for both the Schiff base ligand **(L₁)** and its Cd(II) complex. These calculations, conducted using specific equations, are summarized below [49, 50], providing a comprehensive understanding of the electronic properties and reactivity of the compounds:

$$\mathbf{I = - E_{HOMO}} \quad \mathbf{(1)}$$

$$\mathbf{A = - E_{LUMO}} \quad \mathbf{(2)}$$

$$\mathbf{\Delta E = E_{LUMO} - E_{HOMO}}$$

$$\chi = -\frac{E_{LUMO}+E_{HOMO}}{2} = \frac{I+A}{2} \quad \mathbf{(3)}$$

$$\eta = \frac{E_{LUMO}-E_{HOMO}}{2} = \frac{I-A}{2} \quad \mathbf{(4)}$$

$$w = \frac{(I+A)^2}{4(I-A)} \quad \mathbf{(5)}$$

$$w^- = \frac{(3I+A)^2}{16(I-A)} \quad \mathbf{(6)}$$

$$w^+ = \frac{(I+3A)^2}{16(I-A)} \quad \mathbf{(7)}$$

$$\mathbf{\sigma = 1/\eta} \quad \mathbf{(8)}$$

$$\mathbf{\Delta N_{max} = -I/\eta} \quad \mathbf{(9)}$$

The significance of the energy gap (ΔE) lies in its role as a crucial stability indicator, offering insights into the structural nuances and conformational barriers within various molecular systems. In the case of the Schiff base ligand **(L₁)**, the energy gap measured 8.89 eV, while for the Cd (II) complex, it was determined to be 3.1489 eV. A higher energy gap is indicative of increased stability within the compound. Additionally, it is noteworthy that the chemical potential (Pi) exhibited a negative value, contrasting with the (+ve) value observed for the electrophilicity index (χ). These findings collectively suggest a tendency for the Schiff base ligand to donate electrons to metal ions [51].

TABLE. 6. The numerous optimized and quantum chemical parameters of L_1 its Cd (II) complex.

The calculated quantum chemical parameters	Schiff base ligand (L_1)	[(L_1) (L_2) Cd (Cl)] complex
E (a.u)	-1018.80	-1499.992
Dipole moment (Debye)	3.9111	8.3599
EHOMO (eV)	-7.4355	-5.912222
ELUMO (eV)	1.4609	-2.763318
ΔE (eV)	8.8964	3.148904
χ(eV)	2.9873	4.33777
η(eV)	4.4482	1.574452
$\sigma(eV)^{-1}$	0.22481	0.635141
Pi (eV)	-2.9873	-4.33777
$S\ (eV)^{-1}$	0.112405	0.317570
ω(eV)	1.003098	5.975491
ΔN_{max}	0.671575	2.755098282
Bond lengths (Å)	(L_1)	[(L_1) (L_2) Cd (Cl)]
N(8)-N(9)	1.337	1.350
N(12)-N(13)	1.351	1.412
N(15)-C(16)	1.344	1.380
N(9)-Cd(25)	……	3.401
N(12)-Cd(25)	……	2.440
N(15)-Cd(25)	……	2.375
Cd(25)-Cl(31)		2.484
Bond angles (o)	(L_1)	[(L_1) (L_2) Cd (Cl)]
Cl(31)-Cd(25)-O(27)	……	138.312
Cl(31)-Cd(25)-N(26)	……	103.111
Cl(31)-Cd(25)-N(15)	……	106.096
Cl(31)-Cd(25)-N(12)	……	142.994
Cl(31)-Cd(25)-N(9)	……	101.676
O(27)-Cd(25)-N(26)	……	72.124
O(27)-Cd(25)-N(15)		80.086
O(27)-Cd(25)-N(12)		78.209
O(27)-Cd(25)-N(9)		112.298
N(26)-Cd(25)-N(15)		149.429
N(26)-Cd(25)-N(12)		93.26
N(26)-Cd(25)-N(9)		65.071
N(15)-Cd(25)-N(12)		68.325
N(15)-Cd(25)-N(9)		116.551
N(12)-Cd(25)-N(9)		55.77

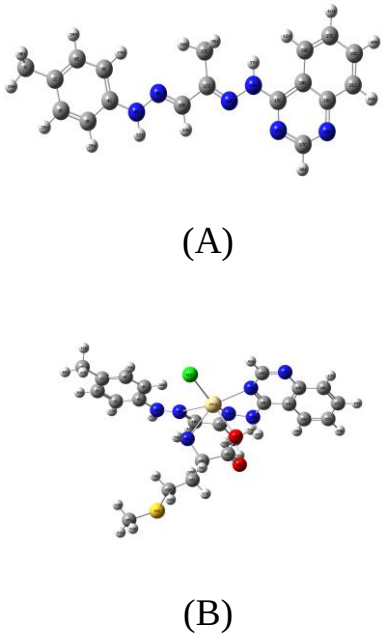

FIGURE 4. The optimized structure of (a) Schiff base ligand **(L_1)** and (b) **[(L_1) (L_2) Cd(Cl)]** complex

3.4. Molecular electrostatic potential (MEP)

To investigate molecular reactions, electrostatic potential V(r) maps were computed to analyse the electronic charge distribution surrounding the molecular surface, aiding in the anticipation of reaction sites [52]. These maps were generated using the same basis set employed for optimization. In this particular investigation, three-dimensional plots of Molecular Electrostatic Potential (MEP) were constructed for both the Schiff base ligand **(L_1)** and its Cd(II) complex (refer to Figure 5). MEP analysis allows the identification of electron-rich regions, indicated by red coloration (favoring sites for electrophilic attack), and electron-poor regions, represented by blue coloration (favoring sites for nucleophilic attack) [53]. Analysis of the MEP maps highlights that regions exhibiting negative potential predominantly involve the electronegative O- and N-atoms. Conversely, regions with positive potential are primarily situated around hydrogen atoms.

Additionally, green-colored regions denote neutral electrostatic potential. The MEP analysis reveals that **(L_1)** exhibits stability with an almost uniform charge distribution. Notably, the electrostatic potential V(r) maps indicate that chelation enhances the potential reaction sites in **(L_1)** complexes.

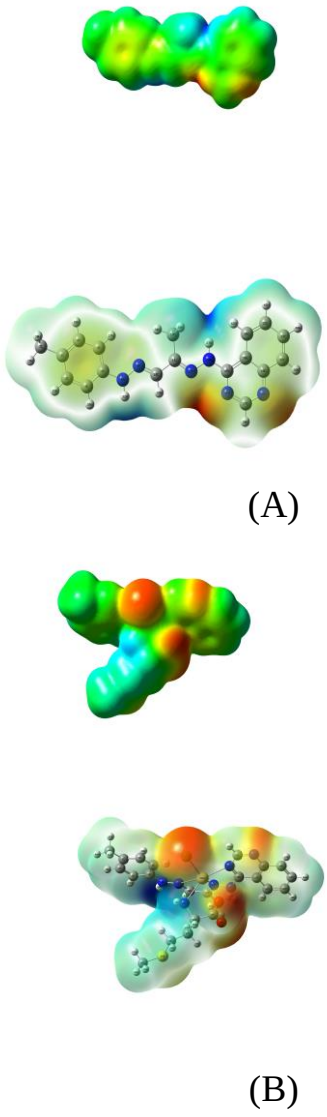

FIGURE 5. Molecular Electrostatic Potential Visualization for (A) Schiff Base Ligand (L_1) and (B) **[(L_1) (L_2) Cd (Cl)]** at an Electron Density Isosurface of 0.004 a.u.

3.5. Antimicrobial activities

The raised effectiveness of metal complexes in battling bacteria contrasted to free Schiff base ligands can be assigned to a crucial process called chelation. During this process, the Schiff base coordinates with metal ions, providing resulting metal chelates with both polar and nonpolar properties [54]. This particular characteristic becomes advantageous as it enables these complexes to penetrate cells and tissues more effectively. When chelation occurs, the metal ion's polarity decreases significantly due to the ligand orbitals overlapping, allowing a partial sharing of the (+ve) charge associated with the metal ion among the donor groups. As a result, chelation causes greater delocalization of π-electrons across the entire chelate ring, thereby enhancing the permeation of the complexes through lipid membranes [55, 56]. Additionally, the chelation process enhances the aqueous and lipid-affinitive properties of the central metal ions, likely contributing to their lipid solubility and their capacity to penetrate the lipid layer of cell membranes. The coordination also modifies the lipophilicity, a factor that influences how quickly molecules can enter cells. Consequently, the altered nature of the metal complex, resulting from coordination, makes it more effective than free ligand [55, 57]. Tests were conducted on the prepared compounds to evaluate their antimicrobial properties against various strains of bacteria and fungi using the disc-agar diffusion method. The assessment encompassed Gram(+ve) bacteria such as Streptococcus mutans and Staphylococcus aureus, Gram(-ve) bacteria comprising Escherichia coli and Klebsiella pneumonia, as well as two strains of fungi - Aspergillus niger and Candida albicans. The detailed findings of these evaluations were tabulated in Table 7 and graphically represented in Figure 6. The data gathered revealed that the Schiff base ligand displayed biological activity against several bacterial species, except for Klebsiella pneumonia and Staphylococcus aureus. The study further delved into the in-vitro (antifungal beside antibacterial) efficacies of both the Schiff base ligand and its metal complexes. For comparison purposes, standard antiseptic, antibiotic, and antifungal drugs like ampicillin, gentamycin, and nystatin, respectively, were used. After conducting a thorough analysis of the biological impacts of Schiff base ligand, metal (II) complexes, and conventional medications, a noteworthy pattern becomes evident: all the metal complexes demonstrate enhanced inhibitory properties against bacterial growth when compared to the uncomplexed ligand. These antibacterial assay results offer several valuable insights:

1. Enhanced Antibacterial Activity: The metal (II) complexes displayed increased efficacy in inhibiting bacterial growth. This suggests that the coordination of the metal ions with the Schiff base ligand may enhance the ligand's inherent antibacterial properties, making it more potent against bacterial strains.
2. Potential for New Antibacterial Agents: These findings indicate that the metal-ligand complexes

have the potential to be developed into novel antibacterial agents. Their superior antibacterial activity suggests that they could be explored as promising candidates for further research and development in the field of antimicrobial drugs.

3. Synergistic Effects: The observed improvements in antibacterial activity in the metal complexes may be attributed to synergistic effects between the metal ions and the ligand. The metal-ligand interactions may lead to more efficient targeting of bacterial cells, resulting in increased inhibition.
4. The complexes are presumed to exhibit antibacterial activity, primarily attributed to the existence of imine groups (-C=N) within the compounds. It is proposed that their mode of action revolves around the establishment of hydrogen bonds facilitated by the azomethine group. This bonding is believed to engage with essential cellular components, potentially disturbing regular cellular processes and thereby enhancing the antibacterial properties of the compounds.
5. Chelation involving M (II) ions leads to a reduction in polarity by neutralizing the positive charge of the metal ion through interaction with ligand-donor groups. Consequently, this phenomenon augments the hydrophobic and lipophilic characteristics of the ligands, thereby promoting their ability to traverse lipid layers in cell membranes. This enhanced permeation may result in the deactivation of enzymes crucial for cellular respiration and the inhibition of protein synthesis, ultimately impeding the growth of organisms.
6. The data indicates that the Cd-complex demonstrates greater toxicity against bacterial species in comparison to the majority of antibiotics in this case ampicillin antibiotic. However, it is noteworthy that its efficacy is lacking in cases where it shows no activity against Streptococcus mutans.
7. The order of effectiveness in terms of antifungal activity against Candida albicans is as follows**: [(L_1) (L_2) Cd (Cl)] > Nystatin > [(L_1) (L_2) Co (Cl)].3H_2O > Schiff base ligand (L_1) > [(L_1) (L_2) Mn (Cl)].2H_2O.**
8. Future Research Opportunities: These results highlight the need for further investigation into the mechanisms of action and structural properties of the metal-ligand complexes. Understanding the underlying factors responsible for the enhanced antibacterial effects can pave the way for the development of more potent antibacterial agents in the future.

Overall, the observations indicate that the complexes formed by combining Schiff base ligands **(L_1)** with metal (II) ions demonstrate heightened antibacterial and antifungal properties compared to their individual constituents. This enhanced efficacy is attributed to distinctive mechanisms of action and chemical characteristics inherent in these complexes. The antibacterial effects are not solely dependent on chelation; rather, they are influenced by a variety of factors.

The effectiveness against microbes is markedly impacted by key elements such as the nature of the metal ion, properties of the ligand, coordination sites, complex geometry, as well as factors like concentration, hydrophobicity, and the presence of co-ligands. It is crucial that the geometric and charge distribution around the substance align with the configuration within bacterial cell wall pores for effective penetration. When this alignment is lacking, the substance cannot enter the wall, compromising compatibility and preventing toxic reactions within the pores. This mismatch may explain the weaker activity observed in certain complexes [58-63].

Furthermore, some observed activities may be attributed to damage incurred during cell wall synthesis, leading to alterations in cell permeability and eventual cell death [64]. In summary, the antibacterial test results reveal that the metal (II) complexes of the Schiff base ligand **(L_1)** exhibit superior inhibitory effects on bacterial growth compared to the uncomplexed ligand, offering exciting possibilities for the development of new antibacterial agents and warranting further research in this area.

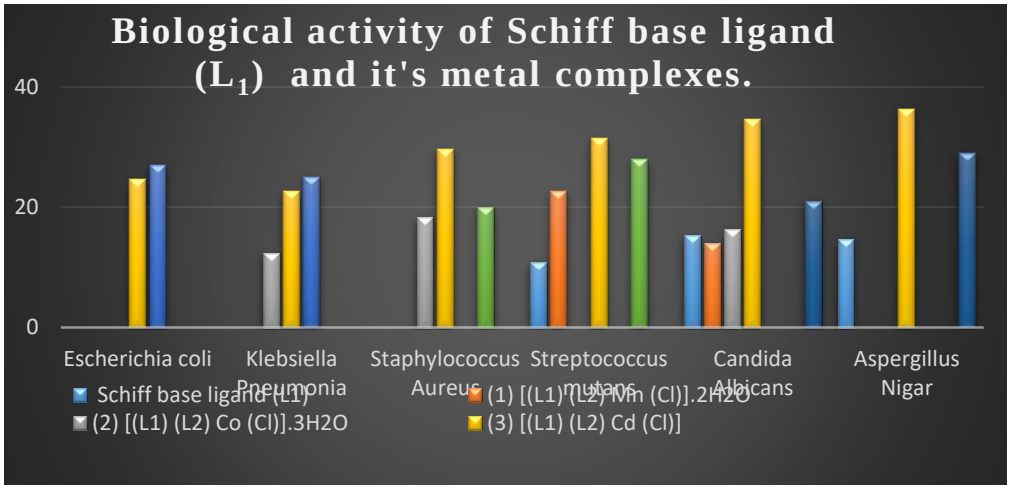

FIGURE. 6. Biological activity of Schiff base ligand **(L_1)** and its metal complexes

Table 7: Biological activity of Schiff base ligand **(L_1)** and its metal complexes.

Sample / Microorganism	Schiff base ligand (L1)	(1) [(L_1) (L_2) Mn (Cl)].2H_2O	(2) [(L_1) (L_2) Co (Cl)].3H_2O	(3) [(L_1) (L_2) Cd (Cl)]	Standard antibiotic
Gram-negative bacterial					**Gentamicin**
***Escherichia coli* (ATCC: 10536)**	**13.9±1.0**	**NA**	**NA**	**24.6±0.6**	**27 ±0.5**
***Klebsiella Pneumonia* (ATCC: 10031)**	**NA**	**NA**	**12.3±0.5**	**22.6±0.6**	**25 ±0.5**
Gram-positive bacteria					**Ampicillin**
***Staphylococcus Aureus* (ATCC: 13565)**	**NA**	**NA**	**18.3±0.5**	**29.6±0.6**	**20 ±0.1**
***Streptococcus mutans* (ATCC: 25175)**	**10.9±0.5**	**22.6±0.6**	**NA**	**31.5±0.6**	**28 ±0.5**
Fungi					**Nystatin**
***Candida Albicans* (ATCC: 10231)**	**15.3±0.5**	**14.0±1.0**	**16.3±0.6**	**34.6±0.6**	**21 ±0.5**
***Aspergillus Nigar* (ATCC: 16404)**	**14.6±0.5**	**NA**	**NA**	**36.3±0.6**	**29±0.5**

3.6. Bioactive Inhibition Targeting H. pylori.

The study aimed to evaluate the inhibitory potential of the Schiff base ligand **(L_1)** and its metal complexes against *H. pylori* by assessing inhibition zones, as illustrated in Table 8 [18]. Furthermore, Table 9 presents the Minimum Inhibitory Concentration (MIC) and Minimum Bactericidal Concentration (MBC) of the Schiff base ligand (**(L_1)**) and its metal complexes (Fig. 7). The MBC/MIC index in Table 9 was utilized to classify the bactericidal or bacteriostatic activity of the samples. A MBC/MIC index ≤ 4 indicated bactericidal activity, whereas an index > 4 suggested bacteriostatic activity [22]. Table 11 demonstrates significant anti-H. pylori activity for all the synthesized compounds Fig 6. In Table 10, it was observed that the efficacy of the synthesized compounds in inhibiting H. pylori varied, with their effectiveness ranked in the following order: **[(L_1) (L_2) Cd (Cl)] > [(L_1) (L_2) Co (Cl)].3H_2O> Schiff base ligand (L_1) > [(L_1) (L_2) Mn (Cl)].2H_2O.** The data indicates that certain artificially created compounds, specifically [**(L_1) (L_2)** Cd (Cl)], demonstrated more pronounced inhibitory effects against H. pylori compared to conventional antibiotics.

This inhibitory action is likely a result of the interaction between the Cd (II) metal center in these Schiff base complex and vital biomolecules within H. pylori, disrupting its metabolic processes and impeding its growth. Consequently, the presence of the Schiff base ligand, along with its coordination with transition metals like Cd (II), seems to confer inhibitory properties against H. pylori. These findings offer promise for the development of innovative therapeutic agents within the realm of chemotherapy. They may potentially serve as alternative or supplementary treatments for H. pylori infections, opening avenues for novel approaches to combatting this bacterium.

Table 8: The diverse inhibitory capacities against H. pylori demonstrated by **L_1** and its related metal complexes.

compounds	Read1	Read2	Read3	Mean	SD	SE
Schiff base Ligand (L_1)	**27**	**26.5**	**26.5**	**26.67**	**0.29**	**0.09**
(1) [(L_1) (L_2) Mn (Cl)].2H_2O	**25**	**25**	**24.5**	**24.83**	**0.29**	**0.09**
(2) [(L_1) (L_2) Co (Cl)].3H_2O	**29**	**30**	**29**	**29.33**	**0.58**	**0.19**
(3) [(L_1) (L_2) Cd (Cl)]	**34**	**34**	**34.5**	**34.17**	**0.29**	**0.09**
Positive Control	**24**	**24**	**24.5**	**24.17**	**0.29**	**0.09**

Table 9: Minimum inhibition and minimum bacteriostatic/bactericidal concentration of Schiff base ligand **(L_1)** and its associated metal complexes against H. pylori.

compounds	MIC (µg/ml)	MBC (µg/ml)	MBC/MIC Index
Schiff base Ligand (L_1)	**62.5**	**62.5**	**1**
(1) [(L_1) (L_2) Mn (Cl)].2H2O	**125**	**250**	**2**
(2) [(L_1) (L_2) Co (Cl)].3H2O	**15.62**	**15.62**	**1**
(3) [(L_1) (L_2) Cd (Cl)]	**125**	**125**	**1**

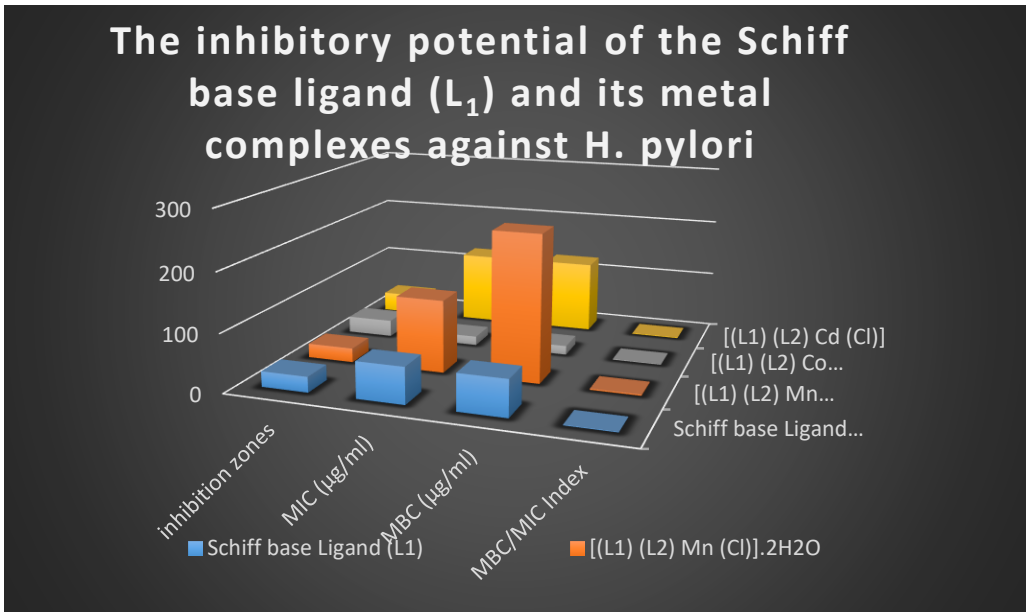

Fig. 7. The inhibitory potential of the Schiff base ligand (L_1) and its metal complexes against *H. pylori*

3.7. Anticancer activities

At present, pharmaceutical research plays a crucial role in the quest for innovative drugs to combat cancer. One significant focus within this field is the exploration of metal-based anticancer compounds. Numerous studies have been conducted to synthesize and assess transition metal complexes for their potential in cancer treatment [65]. In the initial screening process, all produced compounds underwent evaluation towards a breast cancer cell line. Notably, it was observed that **L_1** and the complexes formed with Mn (II), Co (II), and Cd (II) exhibited inhibition fractions exceeding 70% at a concentration of 100 µg/ml, particularly against the MCF-7 cell line.

Furthermore, the active compounds underwent a secondary assessment where their IC_{50} values were determined. This analysis involved varying concentrations (12.5, 25, 50 and 100 µg/ml), as depicted in Figure 8. The results shed light on the potential of these compounds as effective agents in the fight against breast cancer. In a laboratory setting, researchers conducted in vitro investigations to evaluate the cytotoxic effects of a ligand and its complexes on MCF-7 (Breast carcinoma) cells. Survival curves were generated by plotting the relationship between the concentrations of the compounds and the relative viability of the cells. Table 10 presents the IC_{50} values, indicating the concentration at which a 50% inhibition of cancer cell growth occurred. The findings pertaining to cytotoxicity against MCF-7 (Breast carcinoma) cells are summarized as follows:

A) The Schiff base ligand's metal complexes, particularly the Mn(II), Co(II), and Cd(II) derivatives, exhibited notable efficacy against cancer cells, displaying IC_{50} values of 32, 17, and 18 µg/mL, respectively. These outcomes designate these compounds as promising candidates in the field of chemotherapy, as the IC_{50} values represent the concentration required to inhibit 50% of cancer cell growth.

B) The order of effectiveness in chelating metal ions with the ligand can be arranged as **Schiff base Ligand (L_1) < Mn(II) < Cd(III) < Co(II)** when evaluating their impact on MCF-7 cells.

C) A comparative assessment of the antitumor efficacy between the free **L_1** and its metal complexes indicates that the Cobalt (Co) complex demonstrates heightened antitumor activity when contrasted with the ligand itself and its other metal complexes, as detailed in Table 10.

D) The Schiff base ligand **(L_1)** exhibited low cytotoxicity across all tested cancer cell lines, displaying IC_{50} values of 44.5. In contrast, the Co(II) complex demonstrated pronounced cytotoxic effects, with IC_{50} values notably lower at 17.

E) A noticeable association is observed between the anti-tumor and antimicrobial effects. Specifically, the Cd-complex displays heightened antibacterial and antifungal capabilities against the tested bacterial and fungal strains. Concurrently, it demonstrates strong anti-tumor effects on MCF-7 (Breast carcinoma) cells, as detailed in table 8.

F) **The [(L_1) (L_2) Co (Cl)].3H_2O** complex demonstrated superior potency and efficacy relative to the other compounds examined in the study, showing potential as an anticancer drug targeting breast cancer. The superior efficacies of the generated compounds are likely linked to the existence of the azomethine group within the macrocyclic chelate ring. When

metal ions coordinate with the (N) nitrogen atom of the (C=N) group in the chelate ring, there is a reduction in the polarity of the metal atoms. This phenomenon may arise from the partial sharing of the (+ve) charge of the metal ions with the ligand [66–68]. The heightened activity can be assigned to the increased delocalization of π-electron in the ligand upon complex formation. Consequently, the facilitation of complexes permeation across the lipid bilayers of cellular membranes may be enhanced, contributing to their increased efficiency. [69, 70].

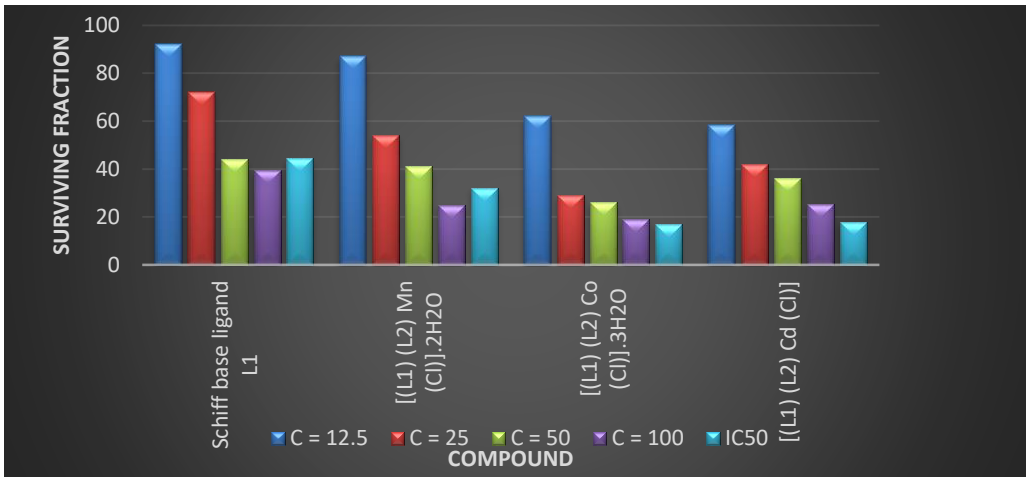

Figure 8. Screening and IC50 Assessment of L1and Metal Complexes on MCF-7 [Breast Cancer Cell Line].

TABLE. 10. Anticancer Efficacy of $\mathbf{L_1}$ and Its Metal Complexes in Combating Breast Cancer.

Compounds	Conc. (µg/mL)				IC50 (µg/mL)
	12.5	25	50	100	
	Surviving fraction (MCF7)				
Ligand (L_1)	**92**	**72**	**44**	**39.5**	**44.5**
(1) [(L_1) (L_2) Mn (Cl)].2H_2O	**87**	**54**	**41**	**25**	**32**
(2) [(L_1) (L_2) Co (Cl)].3H_2O	**62**	**29**	**26**	**19**	**17**
(3) [(L_1) (L_2) Cd (Cl)]	**58**	**42**	**36**	**25.5**	**18**

1. The IC_{50} value, expressed in micrograms per milliliter (µg/ml), represents the concentration of a drug required to hinder the growth of cancer cells by 50%, indicating its cytotoxic effectiveness.

2. The IC_{50} range, measured in µg/ml, classifies the drug's potency into distinct levels: 1-10 (highly potent), 11-20 (potent), 21-50 (moderately potent), 51-100 (mildly potent), and exceeding 100 (non-cytotoxic) [71].
3. Specifically focusing on MCF-7, a subtype of breast carcinoma cell line

3.8. Molecular Docking Investigation of the Schiff Base Ligand (L_1) and its Complex with [(L_1) (L_2) Cd (Cl)].

The examination of potential interaction sites for the Schiff base ligand **(L_1)** and its [**(L_1) (L_2)** Cd (Cl)] **5JEP**), the crystallographic depiction of aberrant oxidoreductase receptors associated with breast cancer (PDB ID: **3HB5**), and the crystal structure of receptor binding domain of the SARS-CoV-2 virus, intricately engaged with the human antibody CR3022 (PDB ID: **6W41**). The computational analysis was carried out using the MOE 2014.09 to describe and predict the binding mode in the pockets of these proteins [72]. The program ran on an Intel(R) Core(TM) i5-7300U CPU @ 2.60GHz 2.70 GHz processor with 16 Giga memory and the Windows 10 operating system. Minimizations were performed with MOE until an RMSD gradient of 0.05 K Cal/mol Å using the MMFF94X force field, and partial charges were automatically calculated. The docking results for (**L_1)** and its **[(L_1) (L_1) Cd (Cl)]** complex are presented in (2D) and (3D) plots in Table 11 and 12, respectively. Additionally, the binding energies for Schiff base ligand **(L_1)** and its Cd (II) complex are provided in Table 13, and for its [**(L_1) (L_2)** Cd (Cl)] complex in Table 14. The experimental findings revealed that the Schiff base ligand **(L_1)** exhibited a noteworthy IC_{50} value of 44.5 µg/ml when tested against a breast cancer cell line. Additionally, the Co(II) and Cd(II) complexes of the ligand demonstrated even greater anticancer activity, displaying the lowest IC_{50} values of 17 µg/ml and 18 µg/ml, respectively. To validate these results, theoretical docking studies were conducted, focusing on the receptors of the breast cancer mutant oxidoreductase with the PDB ID: 3HB5. The docking results indicated that the Schiff base ligand **(L_1)** and its Cd (II) complex exhibited the lowest binding energies of -1.5 and -8.1 kcal mol^{-1}, respectively. This suggests that the complex is more active than its parent ligand, attributed to the formation of coordination bonds with Cd (II) ion. Further investigations into the interactions of these compounds with various outer membrane proteins from bacteria, fungi, and the SARS-CoV-2 receptor revealed significant and effective interactions. The primary interaction forces observed included H-donor, H-acceptor, ionic, and π-H. Of particular note, the Schiff base ligand **(L_1)** and its Cd (II) complex demonstrated the lowest binding energies with receptors **3AHU, 1GHP, 2ZIC, 4N74, 5jpe**, and **6W41**. The ligand exhibited binding energies of NA, −2.5, −1.3, −0.8, −5.9, and −2.1 kcal mol^{-1}, while the Cd (II) complex showed energies of −11.7, −6.9, −8.8, −2.6, −20.1, and −1.7 kcal mol^{-1}, respectively.

Additionally, the coordination was associated with a decrease in binding energy. Consequently, the Cd (II) complex demonstrated higher activity compared to the Schiff base ligand **(L_1)**, suggesting its potential as a highly effective drug against gastroenteritis in the future.

Table 11: Molecular docking 2D and 3D for predicting the possible binding modes of the studied Schiff base ligand **(L_1)** with the receptors of the crystal structure from Protein Data Bank of different types of bacterial species and fungi. In addition, PDB co-crystal form for cancer cell protein

Compound	2D Ligand interaction	3D Ligand interaction		
		Center view	Isolated view	VDW view inside pocket on surface of receptor protein
3AHU	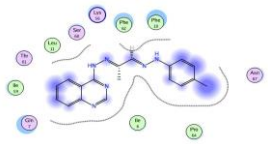	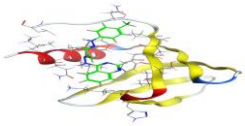	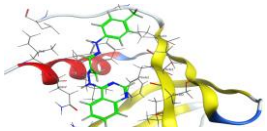	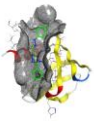
1GHP	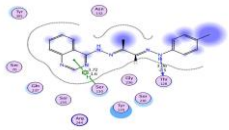	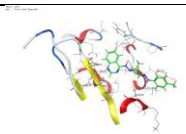	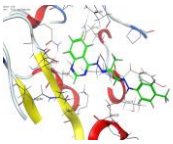	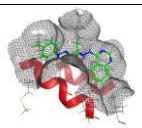
2ZIC	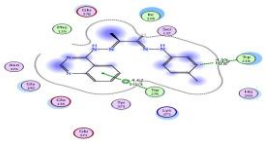	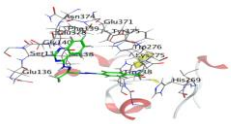	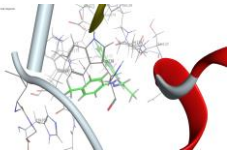	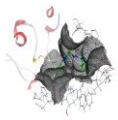
4N74	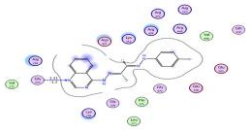	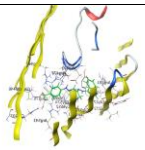	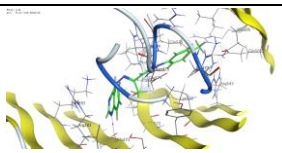	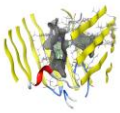
5JPE	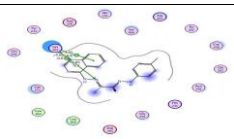	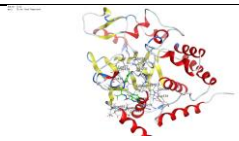	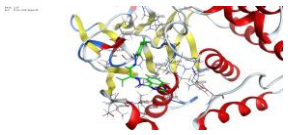	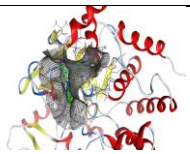
3HB5	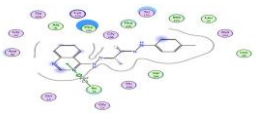	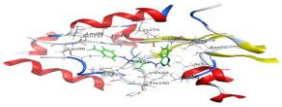	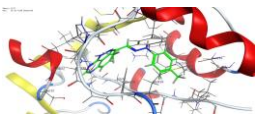	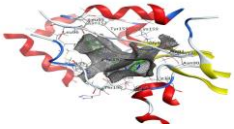
6W41		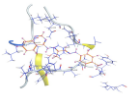	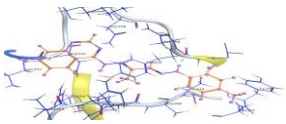	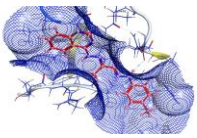

Table 12: Molecular docking 2D and 3D for predicting the possible binding modes of the studied Cd (II) complex with the receptors of the crystal structure from Protein Data Bank of different types of bacterial species and fungi. In addition, PDB co-crystal form for cancer cell protein.

Compound	2D Ligand interaction	3D Ligand interaction		
		Isolated view	Center view	Inside pocket on surface of receptor protein
3AHU	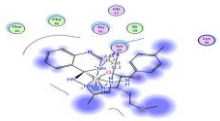	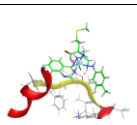	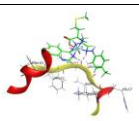	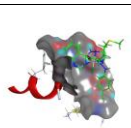
1GHP	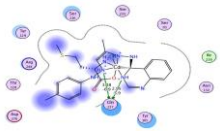	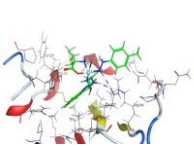	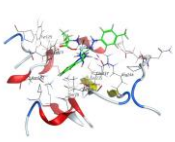	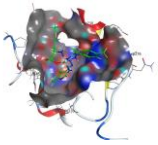
2ZIC	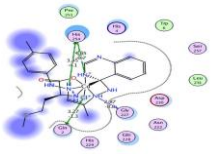	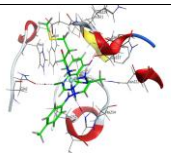		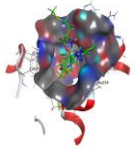
4N74	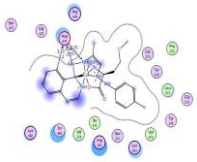	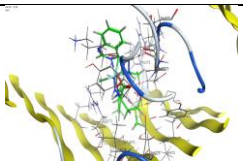		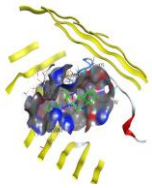
5JPE	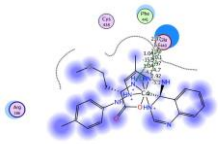	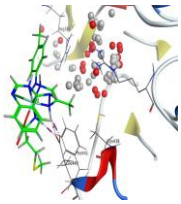		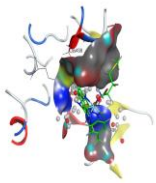
3HB5	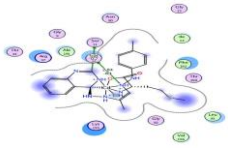	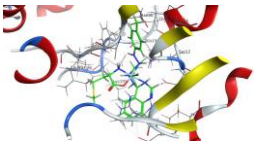	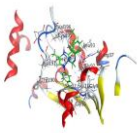	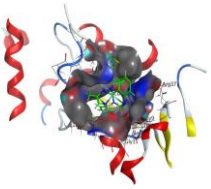
6W41	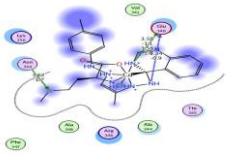	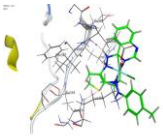	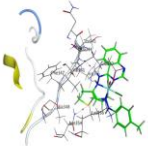	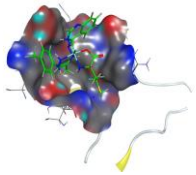

Table 13: Interaction energy values obtained from docking calculations of Schiff base ligand **(L_1)** with different protein receptors

type	Receptor	Ligand moiety	Receptor site	Interaction	Distance (Aº)	E (kcal/mol)
	3AHU	-	-	-	-	-
	1GHP	N 8	O THR 128 (A)	H-donor	3.06	-2.5
G^+ Bacteria		6-ring	OG SER 130 (A)	pi-H	3.72	-1.6
	2ZIC	C 2	6-ring TRP 238 (A)	H-pi	4.55	-0.6
		6-ring	NE1 TRP 276 (A)	pi-H	4.62	-1.3
G^- Bacteria	**4N74**	N 8	CA GLY 273 (A)	H-acceptor	3.33	-1.3
	5jpe	N 12	NZ LYS 263 (A)	H-acceptor	2.83	-5.9
Fungi		6-ring	CD LYS 263 (A)	pi-H	3.69	-0.6
		6-ring	CD LYS 263 (A)	pi-H	4.65	-0.6
Cancer cells	**3HB5**	6-ring	N ILE 14 (X)	pi-H	4.75	-1.5
COVID 19	**6W41**	N 8	O ASN 450 (C)	H-donor	3.02	-2.1
		6-ring	CB SER 349 (C)	pi-H	4.22	-0.9

Table 14: Interaction energy values obtained from docking calculations of Cd (II)-L_1 complex with different protein receptors.

type	Receptor	complex moiety	Receptor site	Interaction	Distance (Aº)	E (kcal/mol)
	3AHU	N 9	O SER 60 (A)	H-donor	3.03	-11.1
		N 17	O SER 60 (A)	H-donor	2.85	-11.7
G^+ Bacteria	**1GHP**	N 9	OE1 GLN 237 (A)	H-donor	3.38	-6.9
		N 17	OE1 GLN 237 (A)	H-donor	2.95	-5.9
	2ZIC	N 9	NE2 HIS 254 (A)	H-donor	3.45	-4.1
		N 13	O GLY 227 (A)	H-donor	2.87	-8.8
		Cl 34	OE1 GLN 2 (A)	H-donor	3.27	-1.3
		N 17	5-ring HIS 254 (A)	cation-pi	4.65	-0.7
G^- Bacteria	**4N74**	N 15	O ASP 473 (A)	H-donor	3.08	-2.6
		C 26	O ASP 473 (A)	H-donor	3.23	-1.2
		N 13	OD2 ASP 473 (A)	ionic	3.73	-1.1
Fungi	**5jpe**	N 13	OE1 GLU 440 (A)	H-donor	2.97	-1.6
		N 13	OE2 GLU 440 (A)	H-donor	2.92	-20.1
		N 29	OE1 GLU 440 (A)	H-donor	3.04	-15.9
		N 13	OE1 GLU 440 (A)	ionic	2.97	-4.7
		N 13	OE2 GLU 440 (A)	ionic	2.97	-5.1

		N 29	OE1 GLU 440 (A)	ionic	3.04	-4.2
Cancer cells	**3HB5**	N 9	OG SER 12 (X)	H-donor	2.84	-8.1
		C 19	OG SER 11 (X)	H-donor	3.32	-0.7
COVID 19	**6W41**	N 15	O GLU 340 (C)	H-donor	3.34	-0.9
		N 17	OE1 GLU 340 (C)	H-donor	3.58	-1.1
		S 37	ND2 ASN 354 (C)	H-acceptor	3.62	-1.7
		N 17	OE1 GLU 340 (C)	ionic	3.58	-1.6

4. Conclusion

This research investigates the properties of the tridentate Schiff base ligand **(L_1)** and its metal (II) complexes using various analytical techniques, such as elemental analysis, molar conductance, mass spectroscopy, IR, and UV-visible spectroscopy. The results of these analyses indicate the formation of octahedral-shaped complexes with Co(II), Cd(II), and Mn(II). The antimicrobial evaluation reveals that the Cd-complex displays significantly higher toxicity against both bacterial and fungal species, comparable to many antibiotics. Additionally, the **(L_1)** Schiff base ligand and its metal complexes, particularly Co(II), Cd(II), and Mn(II), show notable inhibitory effects against H. pylori. The metal complexes of the **(L_1)** Schiff base, especially Mn (II), Co(II) and Cd(II) and demonstrate substantial activity against MCF-7 (Breast carcinoma).

5. References

1. A. Reiss, A. Samide, G. Ciobanu, I. Dabuleanu, Synthesis, spectral characterization and thermal behabior of new metal (II) complexes with Schiff base derived from amoxicillin, J. Chil. Chem. Soc. 60 (2015) 3074.
2. S. Islam, A.K.M.N.A. Siddiki, M.A. Salam, S. Begum, Synthesis, spectral characterization and thermal behaviour of newly derived La(III), Co(III) and Mn(II) complexes with Schiff base derived from methionine and salicylaldehyde, Open J. Inorgc. Chem. 8 (2018) 55.
3. J.R.J. Sorenson, H. Sigel, A review of Metal Ions in Biological System Vol 14 Dekker M, Inc, New York, Basel, p.77.
4. A.M. Abu-Dief, I.M.A. Mohamed, A review on versatile applications of transition metal complexes incorporating Schiff bases Beni-Suff University, J. Bas. App. Sci. 4 (2015) 119.
5. S. Rafique, M. Idress, A. Naim, H. Akbar, A. Athar, A Search for Antibacterial Agents, Biot .Mol. Bio. Review 5 (2010) 38.
6. J.A. Obaleye, A.C. Tella, M.O. Bamigboye, Metal complexes as prospective antibacterial agents, Int. J. Med. Bio. Rech. 27 (2017) 24.
7. R.W. David, Anticancer drug design involving complexes of amino acid and metal ions, Coord. Chem. Review 5 (1972) 123.
8. Pierson, E., Giella, M., & Tishler, M. (1948). Synthesis of DL-methionine. Journal of the American Chemical Society, 70(4), 1450–1451.
9. Willke, T. (2014). Methionine production—a critical review. Applied Microbiology and Biotechnology, 98(24), 9893–9914.
10. Ball, R. O., Courtney-Martin, G., & Pencharz, P. B. (2006). The in vivo sparing of methionine by cysteine in sulfur amino acid requirements in animal models and adult humans. The Journal of Nutrition, 136(6), 1682S-1693S.
11. Krutmann, J., & Humbert, P. (2011). Nutrition for healthy skin. Springer.
12. Soeken, K. L., Lee, W.-L., Bausell, R. B., Agelli, M., & Berman, B. M. (2002). Safety and efficacy of S-adenosylmethionine (SAMe) for osteoarthritis. J Fam Pract, 51(5), 425–430.
13. Prashanthi, Y., & Raj, S. (2009). Synthesis and Characterization of Transition Metal Complexes with. Journal of Scientific Research, 2(1), 114–126. https://doi.org/10.3329/jsr.v2i1.2732
14. Young, S. N., & Shalchi, M. (2005). The effect of methionine and S-adenosylmethionine on S-adenosylmethionine levels in the rat brain. Journal of Psychiatry and Neuroscience, 30(1), 44–48.

15. Lieber, C. S. (2002). S-adenosyl-L-methionine: its role in the treatment of liver disorders. The American Journal of Clinical Nutrition, 76(5), 1183S-1187S.
16. Şerban, G., & Kacso, I. (2020). 2-Amino-1,3,4-Thiadiazole Derivatives As Potential Anti-Helicobacter Pylori Agents-At a Glance. Farmacia, 68(5), 785–791. https://doi.org/10.31925/farmacia.2020.5.3
17. Guideline, A. (2006). Clinical and Laboratory Standards Institute. Wayne, PA, 19.
18. Castillo-Juárez, I., Rivero-Cruz, F., Celis, H., & Romero, I. (2007). Anti-Helicobacter pylori activity of anacardic acids from Amphipterygium adstringens. Journal of Ethnopharmacology, 114(1), 72–77.
19. Frisch, A., Nielson, A. B., & Holder, A. J. (2000). Gaussview user manual. Gaussian Inc., Pittsburgh, PA, 556.
20. French, G. L. (2006). Bactericidal agents in the treatment of MRSA infections—the potential role of daptomycin. Journal of Antimicrobial Chemotherapy, 58(6), 1107–1117.
21. Scott, A. C. (1989). Laboratory control of antimicrobial therapy. Practical Medical Microbiology, 13, 161–181.
22. Malm, A., Glowniak-Lipa, A., Korona-Glowniak, I., & Baj, T. (2015). Anti-Helicobacter pylori activity in vitro of chamomile flowers, coneflower herbs, peppermint leaves and thyme herbs–a preliminary report. Current Issues in Pharmacy and Medical Sciences, 28(1), 30–32.
23. Skehan, P., Storeng, R., Scudiero, D., Monks, A., McMahon, J., Vistica, D., Warren, J. T., Bokesch, H., Kenney, S., & Boyd, M. R. (1990). New colorimetric cytotoxicity assay for anticancer-drug screening. JNCI: Journal of the National Cancer Institute, 82(13), 1107–1112.
24. C. Balakrishnan, L. Subha, M. A. Neelakantan, S. S. Mariappan, Spectrochim. Acta A. 2015, 150, 671.
25. Rehman, W., Yasmeen, R., Rahim, F., & Waseem, M. (2016). CY, Guo, Z. Hassa, U. Rashid, K. J Photochem. Photobiol., B: Biology, 164, 65.
26. Frisch, A., Nielson, A. B., & Holder, A. J. (2000). Gaussview user manual. Gaussian Inc., Pittsburgh, PA, 556.
27. Annaraj, B., Pan, S., Neelakantan, M. A., & Chattaraj, P. K. (2014). DFT study on the ground state and excited state intramolecular proton transfer of propargyl arm containing Schiff bases in solution and gas phases. Computational and Theoretical Chemistry, 1028, 19–26.
28. Geary, W. J. (1971). The use of conductivity measurements in organic solvents for the characterisation of coordination compounds. Coordination Chemistry Reviews, 7(1), 81–122.
29. Rehman, W., Yasmeen, R., Rahim, F., & Waseem, M. (2016). CY, Guo, Z. Hassa, U. Rashid, K. J Photochem. Photobiol., B: Biology, 164, 65.
30. Khan, Z., Maqsood, Z. T., Tanoli, M. A. K., Khan, K. M., Iqbal, L., & Lateef, M. (2015). Synthesis, characterization, in-vitro antimicrobial and antioxidant activities of Co+ 2, Ni+ 2, Cu+ 2 and Zn+ 2 complexes of 3-(2-(2-hydroxy-3-methoxybenzylidene) hydrazono) indolin-2-one. Journal of Basic & Applied Sciences, 11, 125.
31. Abou-Hussein, A. A., & Linert, W. (2014). Synthesis, spectroscopic, coordination and biological activities of some organometallic complexes derived from thio-Schiff base ligands. Spectrochimica Acta Part A: Molecular and Biomolecular Spectroscopy, 117, 763–771.
32. Arafath, M. A., Adam, F., Razali, M. R., Hassan, L. E. A., Ahamed, M. B. K., & Majid, A. M. S. A. (2017). Synthesis, characterization and anticancer studies of Ni (II), Pd (II) and Pt (II) complexes with Schiff base derived from N-methylhydrazinecarbothioamide and 2-hydroxy-5-methoxy-3-nitrobenzaldehyde. Journal of Molecular Structure, 1130, 791–798.
33. Kumar, S., Dhar, D. N., & Saxena, P. N. (2009). Applications of metal complexes of Schiff bases-A review.
34. Tümer, M., Ekinci, D., Tümer, F., & Bulut, A. (2007). Synthesis, characterization and properties of some divalent metal (II)

complexes: Their electrochemical, catalytic, thermal and antimicrobial activity studies. Spectrochimica Acta Part A: Molecular and Biomolecular Spectroscopy, 67(3–4), 916–929.

35. Baošić, R., Radojević, A., Radulović, M., Miletić, S., Natić, M., & Tešić, Ž. (2008). Relationships between structure, retention and biological activity of some Schiff base ligands and their complexes. Biomedical Chromatography, 22(4), 379–386.
36. Kumar, K. S., & Aravindakshan, K. K. (2021). Synthesis, cytotoxic, anticancer and antimicrobial activities of some metal complexes of a novel tetradentate Schiff base ligand,(E)-3-((2-((E)-(1-(2-hydroxyphenyl) ethylidene) amino) ethyl) imino)-N-phenylbutanamide. Results in Chemistry, 3, 100129.
37. Subbaraj, P., Ramu, A., Raman, N., & Dharmaraja, J. (2015). Synthesis, characterization, DNA interaction and pharmacological studies of substituted benzophenone derived Schiff base metal (II) complexes. Journal of Saudi Chemical Society, 19(2), 207–216.
38. Mohammadi, K., Azad, S. S., & Amoozegar, A. (2015). New tetradentate Schiff bases of 2-amino-3, 5-dibromobenzaldehyde with aliphatic diamines and their metal complexes: Synthesis, characterization and thermal stability. Spectrochimica Acta Part A: Molecular and Biomolecular Spectroscopy, 146, 221–227.
39. Mahmoud, W. H., Deghadi, R. G., & Mohamed, G. G. (2017). Preparation, geometric structure, molecular docking thermal and spectroscopic characterization of novel Schiff base ligand and its metal chelates: Screening their anticancer and antimicrobial activities. Journal of Thermal Analysis and Calorimetry, 127, 2149–2171.
40. Mamun, M. A., Ahmed, O., Bakshi, P. K., & Ehsan, M. Q. (2010). Synthesis and spectroscopic, magnetic and cyclic voltammetric characterization of some metal complexes of methionine:[(C5H10NO2S) 2MII]; MII= Mn (II), Co (II), Ni (II), Cu (II), Zn (II), Cd (II) and Hg (II). Journal of Saudi Chemical Society, 14(1), 23–31.
41. Singh, B. K., Rajour, H. K., & Prakash, A. (2012). Synthesis, characterization and biological activity of transition metal complexes with Schiff bases derived from 2-nitrobenzaldehyde with glycine and methionine. Spectrochimica Acta Part A: Molecular and Biomolecular Spectroscopy, 94, 143–151.
42. El-Sonbati, A. Z., Diab, M. A., El-Bindary, A. A., Abou-Dobara, M. I., & Seyam, H. A. (2016). Molecular docking, DNA binding, thermal studies and antimicrobial activities of Schiff base complexes. Journal of Molecular Liquids, 218, 434–456.
43. Frisch, A., Nielson, A. B., & Holder, A. J. (2000). Gaussview user manual. Gaussian Inc., Pittsburgh, PA, 556.
44. Annaraj, B., Pan, S., Neelakantan, M. A., & Chattaraj, P. K. (2014). DFT study on the ground state and excited state intramolecular proton transfer of propargyl arm containing Schiff bases in solution and gas phases. Computational and Theoretical Chemistry, 1028, 19–26.
45. Gupta, M., & Srivastava, M. N. (1985). Synthesis and characterization of mixed ligand complexes of copper (II), nickel (II), cobalt (II) and zinc (II) with glycine and uracil or 2-thiouracil. Polyhedron, 4(3), 475–479.
46. Amudat, L. (2020). Preparation, characterization and antibacterial activity of Mn (II), Cu (II) and Zn (II) complexes of methionine and 2, 2-bipyridine co-ligands.
47. Schlegel, H. B. (1982). Optimization of equilibrium geometries and transition structures. Journal of Computational Chemistry, 3(2), 214–218.
48. Tyagi, P., Tyagi, M., Agrawal, S., Chandra, S., Ojha, H., & Pathak, M. (2017). Synthesis, characterization of 1, 2, 4-triazole Schiff base derived 3d-metal complexes: Induces cytotoxicity in HepG2, MCF-7 cell line, BSA binding fluorescence and DFT study. Spectrochimica Acta Part A: Molecular and Biomolecular Spectroscopy, 171, 246–257.
49. El-Sonbati, A. Z., Mohamed, G. G., El-Bindary, A. A., Hassan, W. M. I., Diab, M. A., Morgan, S. M., & Elkholy, A. K. (2015). Supramolecular structure, molecular docking

and thermal properties of azo dye complexes. Journal of Molecular Liquids, 212, 487–502.
50. Üstün, E., Ayvaz, M. C., Çelebi, M. S., Aşcı, G., Demir, S., & Özdemir, İ. (2016). Structure, CO-releasing property, electrochemistry, DFT calculation, and antioxidant activity of benzimidazole derivative substituted [Mn (CO) 3 (bpy) L] PF6 type novel manganese complexes. Inorganica Chimica Acta, 450, 182–189.
51. Mahmoud, W. H., Mohamed, G. G., & Refat, A. M. (2017). Preparation, characterization, biological activity, density functional theory calculations and molecular docking of chelates of diazo ligand derived from m-phenylenediamine and p-chlorophenol. Applied Organometallic Chemistry, 31(11), e3753.
52. El-Bindary, M. A., & El-Bindary, A. A. (2022). Synthesis, characterization, DNA binding, and biological action of dimedone arylhydrazone chelates. Applied Organometallic Chemistry, 36(4), e6576.
53. un Nisa, Z., Gul, A., Akhter, Z., Nadeem, M. A., Tahir, M. N., & Ahmed, M. U. (2016). Some newly synthesized ferrocene based esters: Characterization, DNA interaction and DFT studies. Journal of Organometallic Chemistry, 820, 130–140.
54. Joseyphus, R. S., & Nair, M. S. (2008). Antibacterial and antifungal studies on some schiff base complexes of zinc (II). Mycobiology, 36(2), 93–98.
55. Mahmoud, W. H., Deghadi, R. G., & Mohamed, G. G. (2017). Preparation, geometric structure, molecular docking thermal and spectroscopic characterization of novel Schiff base ligand and its metal chelates: Screening their anticancer and antimicrobial activities. Journal of Thermal Analysis and Calorimetry, 127, 2149–2171.
56. Neelakantan, M. A., Marriappan, S. S., Dharmaraja, J., Jeyakumar, T., & Muthukumaran, K. (2008). Spectral, XRD, SEM and biological activities of transition metal complexes of polydentate ligands containing thiazole moiety. Spectrochimica Acta Part A: Molecular and Biomolecular Spectroscopy, 71(2), 628–635.
57. Mahmoud, W. H., Sayed, F. N., & Mohamed, G. G. (2016). Synthesis, characterization and in vitro antimicrobial and anti-breast cancer activity studies of metal complexes of novel pentadentate azo dye ligand. Applied Organometallic Chemistry, 30(11), 959–973.
58. Osowole, A. A. (2008). Syntheses and characterization of some tetradentate Schiff-base complexes and their heteroleptic analogues. E-Journal of Chemistry, 5(1), 130–135.
59. Osowole, A. A., Kolawole, G. A., & Fagade, O. E. (2008). Synthesis, characterization and biological studies on unsymmetrical Schiff-base complexes of nickel (II), copper (II) and zinc (II) and adducts with 2, 2′-dipyridine and 1, 10-phenanthroline. Journal of Coordination Chemistry, 61(7), 1046–1055.
60. Bansod, A., Bhaskar, R., Ladole, C., Salunkhe, N., Thakare, K., & Aswar, A. (2022). Synthesis, Characterization, Biological Activity and Solid-State Electrical Conductivity Study of Some Metal Complexes Involving Pyrazine-2-Carbohydrazone of 2-Hydroxyacetophenone. Journal of Transition Metal Complexes, 5.
61. Manjuraj, T., Yuvaraj, T. C. M., Jayanna, N. D., & Sarvajith, M. S. (2022). Design, spectral, thermal, DFT studies, antioxidant and molecular docking studies of pyrazole-based schiff base ligand and its metal (II) complexes. Materials Today: Proceedings, 54, 646–655.
62. El-Gammal, O. A., El-Bindary, A. A., Mohamed, F. S., Rezk, G. N., & El-Bindary, M. A. (2022). Synthesis, characterization, design, molecular docking, anti COVID-19 activity, DFT calculations of novel Schiff base with some transition metal complexes. Journal of Molecular Liquids, 346, 117850.
63. Alharbi, A., Alzahrani, S., Alkhatib, F., Al-Ola, K. A., Alfi, A. A., Zaky, R., & El-Metwaly, N. M. (2021). Studies on new Schiff base complexes synthesized from d10 metal ions: Spectral, conductometric measurements, DFT and docking simulation. Journal of Molecular Liquids, 334, 116148.
64. Iftikhar, B., Javed, K., Khan, M. S. U., Akhter, Z., Mirza, B., & Mckee, V. (2018). Synthesis, characterization and biological assay of Salicylaldehyde Schiff base Cu (II) complexes and their precursors. Journal of Molecular Structure, 1155, 337–348.

65. Ebrahimipour, S. Y., Sheikhshoaie, I., Castro, J., Haase, W., Mohamadi, M., Foro, S., Sheikhshoaie, M., & Esmaeili-Mahani, S. (2015). A novel cationic copper (II) Schiff base complex: Synthesis, characterization, crystal structure, electrochemical evaluation, anti-cancer activity, and preparation of its metal oxide nanoparticles. Inorganica Chimica Acta, 430, 245–252.
66. Zafar, H., Kareem, A., Sherwani, A., Mohammad, O., Ansari, M. A., Khan, H. M., & Khan, T. A. (2015). Synthesis and characterization of Schiff base octaazamacrocyclic complexes and their biological studies. Journal of Photochemistry and Photobiology B: Biology, 142, 8–19.
67. Khan, T. A., Naseem, S., Hajra, R., & Shakir, M. (2010). Synthesis, Physicochemical, and Antimicrobial Screening Studies of Complexes of Co (II), Ni (II), Cu (II), and Zn (II) with 18-membered Schiff Base Octaazamacrocyclic Ligand. Synthesis and Reactivity in Inorganic, Metal-Organic, and Nano-Metal Chemistry, 40(10), 861–868.
68. Cotton, F. A., Wilkinson, G., Murillo, C. A., & Bochmann, M. (1999). Advanced inorganic chemistry. John Wiley & Sons.
69. El-Boraey, H. A., & El-Din, A. A. S. (2014). Transition metal complexes of a new 15-membered [N5] penta-azamacrocyclic ligand with their spectral and anticancer studies. Spectrochimica Acta Part A: Molecular and Biomolecular Spectroscopy, 132, 663–671.
70. Qian-Qian, Z. Bin, Chinese J. Str. Chem. 2012, 31(4), 555.
71. Mosmann, T. (1983). Rapid colorimetric assay for cellular growth and survival: application to proliferation and cytotoxicity assays. Journal of Immunological Methods, 65(1–2), 55–63.
72. Vilar, S., Cozza, G., & Moro, S. (2008). Medicinal chemistry and the molecular operating environment (MOE): application of QSAR and molecular docking to drug discovery. Current Topics in Medicinal Chemistry, 8(18), 1555–1572.